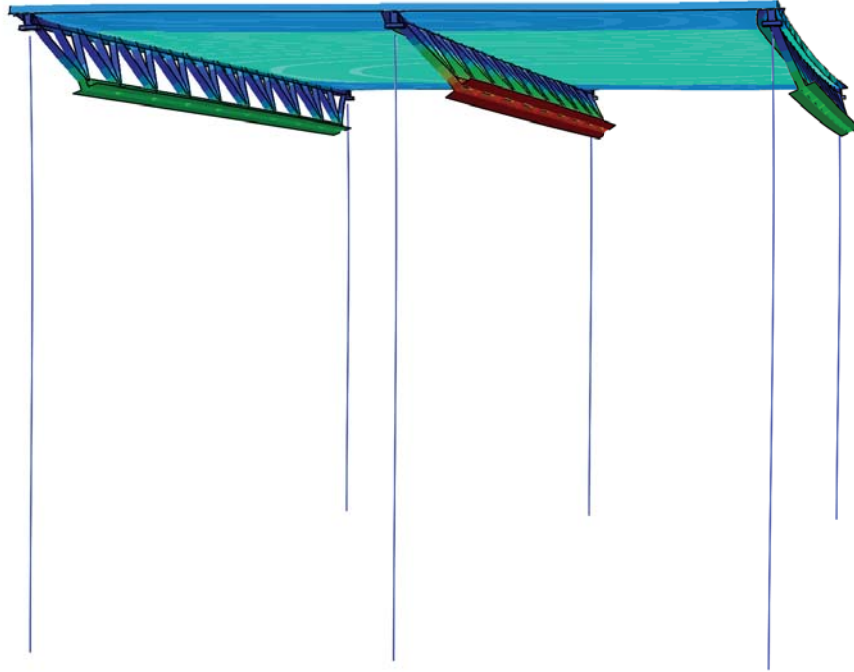




LUND
UNIVERSITY



STEEL TRUSSES IN INDUSTRIAL BUILDINGS

Load Bearing Capacity and Lateral Buckling Resistance

ADAM EL-SHERIF and HANNA GARDSHOL

Structural
Mechanics

Master's Dissertation

DEPARTMENT OF CONSTRUCTION SCIENCES
DIVISION OF STRUCTURAL MECHANICS

ISRN LUTVDG/TVSM--24/5274--SE (1-81) | ISSN 0281-6679

MASTER'S DISSERTATION

STEEL TRUSSES IN INDUSTRIAL BUILDINGS

Load Bearing Capacity and Lateral Buckling Resistance

ADAM EL-SHERIF and HANNA GARDSHOL

Supervisors: Professor **ERIK SERRANO**, Division of Structural Mechanics, LTH
and **ARASH ROOHBAKHSH**, Senior Structural Engineer, AFRY.

Examiner: **HENRIK DANIELSSON**, Associate Professor, Division of Structural Mechanics, LTH.

Copyright © 2024 Division of Structural Mechanics,
Faculty of Engineering LTH, Lund University, Sweden.

Printed by V-husets tryckeri LTH, Lund, Sweden, June 2024 (PI).

For information, address:

Division of Structural Mechanics,
Faculty of Engineering LTH, Lund University, Box 118, SE-221 00 Lund, Sweden.

Homepage: www.byggmek.lth.se

Abstract

The dissertation deals with the load-bearing capacity, in terms of stability, of a steel truss in an industrial building. It is based on previous work by Tosovic [1], in which the roof was investigated in the same type of building but the results showed that the trusses were the deficient elements.

Steel trusses are a popular choice of construction for large-span buildings due to their load-bearing capacity over large spans. However, collapse of the building type has occurred on several occasions in recent years, especially in northern Sweden, whereby faulty construction and high snow loads have been identified as potential causes of the collapse. A common truss construction in the Nordic countries was selected for the analysis. The methodology used Abaqus, a finite element analysis software. Initially, an investigation of modelling methods was carried out with a smaller truss, the purpose of which was to find a model that provided increased efficiency in modelling without sacrificing accuracy in the result.

Using the developed modelling method, the truss was initially constructed with the columns and their connections. The result provided insight into the slenderness and buckling behaviour of the truss. By using Eurocode 3, the reduction factor of the truss was obtained in relation to the theoretical bearing capacity of the material strength.

An industrial building with three trusses and a corrugated steel roof was designed and simulations with three different load cases were used to analyse the behaviour of the building. The first case involved a uniformly distributed load over the entire roof. The other two had a distributed load on half the roof and a horizontal load on one truss to initiate second-order effects. Contrary to previous work by Tosovic [1], all results showed that the roof yielded before the truss. A thicker roof was investigated for all load cases to eliminate eigenvalues when the roof buckles. The result gave an eigenvalue for each case where the trusses buckle.

A parametric study was carried out with a model of a truss using springs along the theoretical connection of the truss to the roof. The study investigated the influence of different spring axial stiffness perpendicular to the truss direction and rotational stiffness around the truss. These are mainly stabilised degrees of freedom by the roof.

The results show that the truss's design moment capacity, without a roof, can only be utilised about 10%. The reduction factor increased drastically to about 60% when the whole building was examined with a thicker roof.

The parametric study displayed how the axial stiffness of a roof has a greater impact than rotational stiffness on the stability of the structure, along with the influence of rotational stiffness decreasing with higher axial stiffness. Due to difficulties in obtaining values from the buckling analysis, an alternative static analysis was performed where boundary conditions replaced the springs. It resulted in reduction right below 50%.

Sammanfattning

Arbetet behandlar bärförmåga, med avseende på stabilitet, hos ett stålfackverk i en industriell byggnad. Det baseras på tidigare arbete av Tosovic [1], där taket undersöktes i samma typ av byggnad men resultatet visade att fackverken var de bristande beståndsdelarna.

Stålfackverk är ett populärt val av konstruktion vid öppna planlösningar tack vare deras bärförmåga över stora spännvidder. Däremot har kollaps av byggnadstypen varit förekommande vid flertalet tillfällen de senaste åren framförallt i norra Sverige, varpå felaktig konstruktion och hög snölast pekats ut som potentiella orsaker till rasen.

En vanlig fackverskonstruktion i Norden valdes ut för analyserna. I metoden användes Abaqus, en programvara inom finita elementanalyser. Initiellt utfördes en undersökning av modelleringsmetoder med ett mindre fackverk, vars syfte var att hitta en modell som gav ökad effektivitet i modellerandet utan att uppoffra noggrannhet i resultatet.

Med den framtagna modelleringsmetoden konstruerades inledningsvis fackverket ihop med pelarna och dess anslutningar. Resultatet gav insikt i fackverkets slankhet och knäckningsbeteende. Genom användning av Eurocode 3 erhöles fackverkets nyttjandegrad i förhållande till teoretisk bärförmåga avseende materialets hållfasthet.

En industriell byggnad med tre fackverk och korrugerat ståltak togs fram varpå simuleringar med tre olika lastfall användes för att analysera byggnadens beteende. Första fallet innebar en jämnt utbredd last över hela taket. De två övriga hade en utbredd last på halva taket samt en horisontell last på ett fackverk för att initiera andra ordningens effekter. I motsats till tidigare arbete av Tosovic [1] visade samtliga resultat att taket gav efter innan fackverket. En version med tjockare tak undersöktes hos samtliga lastfall för att eliminera vissa egenvärden då taket knäcks. Resultatet gav ett egenvärde för varje fall där fackverken knäcks.

Slutligen genomfördes en parameterstudie med en modell av ett fackverk där fjädrar längs fackverkets teoretiska koppling till taket användes. Studien undersökte påverkan av olika fjäderstyvheter tvärs i fackverkets riktning samt rotationsstyvhet kring fackverket, vilka är de frihetsgrader som taket främst stabiliserar.

Resultatet visar att fackverket, utan tak, har en reduktionsfaktor på cirka 10% innan instabilitet. Reduktionsfaktorn ökade drastiskt till cirka 60% för det kritiska då hela bygganden undersöktes med tjockare tak.

Parameterstudien visade att takplåtens axialstyvhet hade en större inverkan på stabiliteten hos strukturen än rotationsstyvhet. Vidare visade resultatet att inverkan av rotationsstyvheten minskade med högre axialstyvhet. Då svårigheter att erhålla värden från bucklingsanalysen uppstod utfärdades en alternativ statisk analys där randvillkor ersatte fjädrarna. Resultatet uppvisade en reduktionsfaktor strax under 50%.

Acknowledgements

We wish to express our gratitude to our supervisors Erik Serrano and Arash Roohbakhsh for their valuable assistance and insights throughout the progression of this project. Their guidance has played a pivotal role in shaping our approach and navigating the challenges we encountered along the way. Their commitment to our development and the project's success has not only encouraged our academic growth but also ensured the attainment of our goals.

We would also extend our thanks to our examiner, Henrik Danielsson, for his contributions and feedback, which have provided us with perspectives and considerations regarding our work.

Notations and Symbols

Latin letters

A - Area

\mathbf{a} - Global displacement vector

\mathbf{a}^e - Nodal displacement vector

\mathbf{B} - Derivatives of shape functions

\mathbf{b} - Body force vector

\mathbf{D} - Constitutive matrix

E - Modulus of elasticity

F_{cr} - Critical buckling load

F_{Ed} - Design load

\mathbf{f} - Global force vector

\mathbf{f}^e - Element force vector of \mathbf{f}

\mathbf{f}_0 - Initial strain vector of \mathbf{f}

\mathbf{f}_b - Boundary vector of \mathbf{f}

\mathbf{f}_l - Load vector

f_y - Yield Strength

H - Height

h - Traction vector of essential boundary conditions

I - Moment of inertia

\mathbf{K} - Global stiffness matrix

\mathbf{K}^e - Element stiffness matrix

\mathbf{K}_0 - Initial stiffness matrix

\mathbf{K}_Δ - Geometric stiffness matrix induced by internal axial forces from the external loads due to the incremental loading pattern of the buckling step

\mathbf{K}_λ - Geometric stiffness matrix including effects internal forces

\mathbf{K}_σ - Geometric stiffness matrix including effects of displacements

k - Stiffness

k_a - Axial stiffness

k_r - Rotational stiffness

L - Length

M_{cr} - Critical buckling moment

M_{Rd} - Design moment resistance

\mathbf{N} - Shape functions

P - Force at node

r - Residual

t - Traction vector of natural boundary conditions

u - Displacement

v - Mode Shape

q_{cr} - Critical buckling load

q_g - Self-weight

q_{live} - Live load

q_{Rd} - Design load resistance

Greek letters

α_{cr} - Critical design load factor

α_{LT} - Imperfection factor for lateral-torsional buckling

ϵ_0 - Initial strains

λ - Eigenvalue

ν - Poissons ration

$\bar{\lambda}_{LT}$ - Non-dimensional slenderness for lateral torsional buckling

ρ - Density

ϕ_{LT} - Value to determine the reduction factor χ_{LT}

χ_{LT} - Reduction factor for lateral-torsional buckling

Contents

Abstract	I
Sammanfattning	III
Acknowledgements	V
Notations and Symbols	VII
Table of Contents	XI
1 Introduction	1
1.1 Collapses of Industrial Building	1
1.2 Steel Trusses	1
1.3 Investigated Structure	2
1.4 Aim and Objectives	3
1.5 Limitations	4
2 Theory	5
2.1 Steel as a Building Material	5
2.2 Eurocode 3	5
2.3 Finite Element Method	8
2.3.1 Overview	8
2.3.2 Description of the Finite Element Method	8
2.3.3 Nonlinear Analysis	9
2.3.4 Analysis Procedures	11
2.3.5 Modelling Elements	12
2.4 Abaqus FEA	14
2.4.1 Overview	14
2.4.2 Part	15
2.4.3 Property	15
2.4.4 Assembly	16
2.4.5 Step	16
2.4.6 Interaction	17
2.4.7 Load	19
2.4.8 Mesh	20
3 Modelling Approaches	21
3.1 Method	21
3.1.1 Simplified Model	21
3.1.2 Property Definition	22

IX

3.1.3	Load and Boundary conditions	23
3.1.4	Step and mesh	23
3.1.5	Model A	24
3.1.6	Model B	25
3.1.7	Model C	25
3.1.8	Model D	26
3.1.9	Mesh Convergence Analysis	26
3.2	Results	27
3.2.1	Deflections	27
3.2.2	Choice of model	28
3.2.3	Mesh Element Size	29
4	Analysis of an Industrial Building	31
4.1	Description of Industrial Building	31
4.1.1	Components	31
4.1.2	Dimensions	33
4.2	Abaqus Model	33
4.2.1	Truss	34
4.2.2	Connection of Truss to Column	34
4.2.3	CGI Roof	35
4.2.4	Boundary Conditions	36
4.2.5	Load Definitions	37
4.3	Trials	37
4.3.1	One Truss	37
4.3.2	Industrial Building with Three Trusses	39
4.3.3	Parametric Study of One Truss	40
4.3.4	Alternative Modelling Approaches	43
4.4	Results	44
4.4.1	One Truss	44
4.4.2	Industrial building with three trusses	44
4.4.3	Parametric Study of One Truss	47
4.4.4	Alternative Modelling Approaches	53
5	Discussion	55
5.1	Single Truss	55
5.2	Industrial Building	55
5.3	Parametric Study of One Truss	56
5.4	Alternative Modelling Approaches	59
5.5	Usage of Line Elements	59
5.6	Contribution to Previous Research	60
6	Conclusion	61
6.1	Buckling Resistance of the Truss	61
6.2	Load Capacity of Industrial Building	61
6.3	Modelling Approach	62
6.4	Continued Research	62
	Bibliography	63

A Detail Drawings from MAKU	65
B Detail Drawings from Ruukki	67
C All Result from Parametric Study	71

1 Introduction

1.1 Collapses of Industrial Building

During the last few years, reports regarding collapses of industrial buildings in Sweden have been reoccurring. In February of 2024, multiple buildings were reported as having collapsed. Most occurrences were in the northern parts of the country during periods of heavy snow, which has been identified as a possible cause in most cases. However, investigations show that the snow loads rarely exceed the design load. The underlying issue therefore seems to rather be an effect of either inadequate construction during assembly or insufficient stability of the structure itself.

Construction of industrial buildings often includes large spans of load-bearing components due to the requirements of substantial open spaces. Commonly, steel trusses along with a corrugated roof are used as load-bearing components.

1.2 Steel Trusses

In Swedish construction, the use of steel trusses is a key feature. Known for their strength and adaptability, steel trusses play a big role in the architecture of industrial facilities across the country. Steel trusses are favoured because of their ability to span large distances, providing open and flexible floor plans. The durability of steel makes it well-suited for Sweden's varied weather conditions where the material ensures safety and longevity.

Steel trusses are used in various applications ranging from sports arena roofs to airport terminals thanks to their structural ability and cost-effectiveness. Compared to alternatives like I- and H-sections, steel trusses are lightweight yet stiff, resulting in smaller deflection under load. It also makes them suitable for transferring loads to connected structures in multi-storey buildings. [2]

Designing a steel truss involves selecting an appropriate structural form, where factors such as safety, construction, cost-effectiveness and structural performance need to be considered. The primary principle in form selection is to ensure that longer steel elements are primarily exposed to tension, while shorter elements bear compression. This requires an analysis of all design load scenarios and combinations, with the most critical load combination dictating the decision-making of the structural form.

Trusses are assemblies of straight members interconnected at each end, typically through pin joints. These joints are often created by bolting or welding and should aim at reducing moments at the connections. External loads on the trusses are assumed to act solely at the joints, making all members subjected to only axial forces, either

compression or tension, without bending moments or shear forces. Consequently, truss members experience uniform stress distribution, enabling lighter elements with higher load capacity and efficient cross-sectional usage. [3]

1.3 Investigated Structure

An industrial building specified by the company AFRY was used in the analysis, where the construction of the truss follows a common Nordic design used by the company. Its load-bearing components could be divided into three major components: the corrugated roof, the trusses, and the columns. All components are made of steel. A version of a building with three trusses can be seen in Figure 1.1.

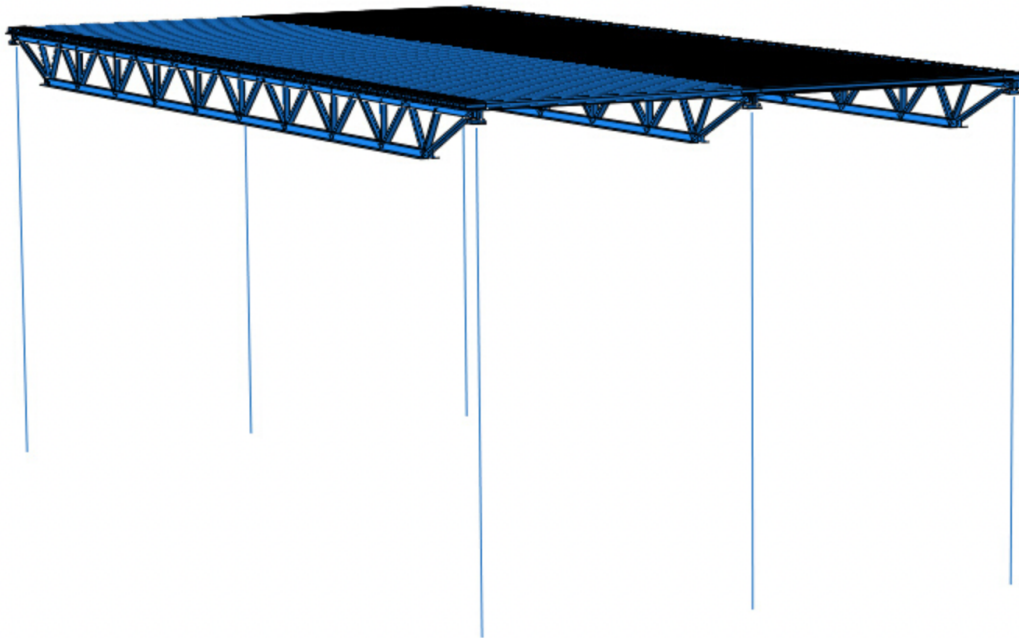


Figure 1.1: Model of the industrial building created in Abaqus where three trusses have been used.

The modelled roof of the building was corrugated galvanised steel (CGI) plates. The corrugated design offers superior bending stiffness and allows for increased load-bearing capacity over larger spans without compromising structural integrity. The pattern utilises the material steel which takes tension and torsion forces well, this provides added resistance against bending and deformation in all directions. The feature is advantageous for heavy snowfalls or high winds and helps maintain stability and longevity for the roof. CGI plate's ability to withstand greater loads and spans makes them a suitable option for industrial buildings. Furthermore, they are easy to install and cost-effective since material use is minimised. In the building investigated, the crests of the corrugated roof, in which direction the largest stiffness is found, are directed perpendicular to the truss, see Figure 1.2. Thus, the roof counteracts the buckling of the trusses more efficiently when subjected to compressive forces on the roof.

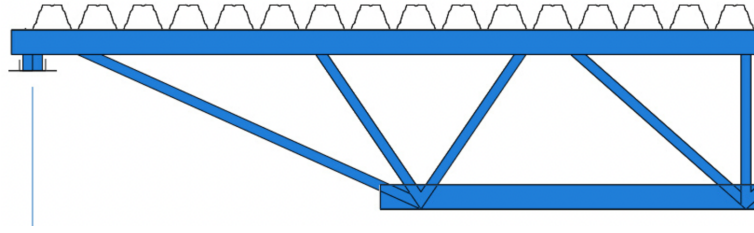


Figure 1.2: Directions of roof in relation to the trusses.

Previous work has been done on the building by Tosovic [1], where the corrugated roof was investigated as it was believed to be the weakest load-bearing component. The model was created in the finite element analysis software Abaqus where mostly beam elements were used when modelling the building. The corrugated roof was the only exception, made of shell elements. The result of the report disproved the hypothesis, as the truss seemed to buckle before the roof.

To continue the previous research by Tosovic [1], this dissertation focuses on the steel trusses of the industrial building.

1.4 Aim and Objectives

This work aims to investigate the load-bearing capacity of the steel trusses of an industrial building. Aspects considered include lateral buckling conditions and varying loading circumstances.

A major focus of the dissertation has been spent on simulating the contributing parameters caused by the construction of the building. It includes parameters such as how the truss has been assembled, how the truss is connected to the columns, and how the components interact in transferring the forces.

To obtain a realistic model in Abaqus, emphasis has been put on modelling the mentioned parameters as close to reality as possible. Thus, the work included investigating assembling approaches of the truss, along with experimenting with different tools in the software.

To summarise, the main objectives are to:

1. Obtain an appropriate modelling approach when using Abaqus for simulations.
2. Evaluate the rotational buckling resistance of the steel trusses in the industrial building, regarding the trapezoidal plates and varying load conditions.
3. Estimate the influence of a roof's stiffness on the buckling behaviour and resistance of the truss through a parametric study.

1.5 Limitations

The geometry of the construction in terms of for instance lengths, cross-sections, and selection of truss and roof structure from manufacturers were kept consistent throughout the analysis. The only investigation conducted on changing a component of the construction was of the stiffness caused by an overhead construction on the trusses in the parametric study.

As the analysis focused on the capacity of the truss in combination with other structural components, steel quality remained consistent throughout the analysis.

Climate conditions such as changes in temperature were neglected.

The model was created using shell elements for all components except the columns where line elements were used. A comparison between neither the selection of elements nor mesh geometry was made.

Boundary conditions of the columns in relation to ground and surrounding construction were not varied.

The parametric study was limited to investigating the effect of the stiffness of the spring by varying the axial stiffness in one direction and the rotational stiffness in one direction. Both selected parameters were assumed to impose the largest effect on the truss.

2 Theory

2.1 Steel as a Building Material

Steel is a versatile material that is applied in a wide range of fields in construction. With numerous types of steel available, along with diverse standards and regulations governing parameters such as connections, forms and surface treatments, the material provides unique construction opportunities. The complexity further increases due to advanced production processes and material quantities, making steel highly innovative and complex. Unlike composite materials like reinforced concrete, steel has high compressive and tensile strength even without combining it with other materials. [4]

When prefabricated off-site, structural steel offers the advantage of immediate erection upon arrival at the project site. This eliminates the need for formwork and generally requires minimal to no shoring for structural steel-framed projects. The mounting can take place in nearly any weather condition and is not restricted by specific temperature requirements. This accelerates construction timelines, reduces on-site labour needs, and lowers the overall project costs.

Structural steel enables long spans and open, column-free spaces, because of its high strength-to-weight ratio. Compared to concrete, structural steel significantly reduces the weight needed to support the same load requirements. The strength of steel in both tension and compression, and its ability to bend without cracking or breaking stands out from other building materials. It does not experience creep under load over time.

Industrial buildings belong to the most common type of steel buildings. A prominent challenge when designing the building type includes large spans, where steel is favourably used. Because of its low column footprint, steel allows increased usable floor space and greater design flexibility while minimising material usage. [5]

2.2 Eurocode 3

Eurocode is a set of European standards governing the design and construction of civil engineering works. Developed by the European Committee for Standardisation it provides unified guidelines to ensure the safety, durability, and efficiency of structures across Europe. This dissertation mainly focuses on chapters 5 and 6 in EN 1993: Eurocode 3 - Design of steel structures.

This dissertation will include equations from EN:1993-1-1:2005 *Eurocode 3: Design of Steel Structures* to calculate the reduction factor of the lower chord of the truss.

Chapter 5 of EN:1993-1-1:2005 named *Structural Analysis* stands as a document guiding the design of structural steel elements. Material properties are a crucial part of this chapter where parameters such as yield strength and ductility are covered and guide the selection of appropriate steel elements. The cross-section requirements of steel elements are also addressed regarding the classification and resistance of cross-sections. The classification of the cross-section is based on the steel members' structural shape and behaviour. By this categorisation according to the predefined criteria such as compactness, slenderness and geometric properties, engineers are provided with a structured approach to optimise the efficiency and performance of steel elements. Chapter 5 addresses what kind of analysis engineers should be making based on Equations 2.1 and 2.2

$$\alpha_{cr} = \frac{F_{Cr}}{F_{Ed}} \geq 10 \quad \text{for elastic analysis} \quad (2.1)$$

$$\alpha_{cr} = \frac{F_{Cr}}{F_{Ed}} \geq 15 \quad \text{for plastic analysis} \quad (2.2)$$

where α_{Cr} is the critical design load factor, F_{Cr} is the buckling load, and F_{Ed} is the design load acting on the structure.

For elastic analysis where the structure is assumed to behave linearly within its elastic range, Eurocode specifies that the critical design load factor should be equal to or greater than 10. This criterion ensures that the design loading is sufficiently lower than the critical buckling load to prevent elastic instability or buckling under applied loads. Consequently, the structure remains within its elastic limits and does not experience premature failure due to buckling along with geometric deformations having no significant effect on the analysis results.

Plastic analysis considers the nonlinear behaviour of the structure due to material plasticity and allows the redistribution of internal forces beyond the elastic limit. For this, the Eurocode specifies a higher threshold for the slenderness ratio, where it should be equal to or greater than 15. This criterion reflects the increased robustness required for plastic analysis where the structure failure mechanisms may differ from those under purely elastic conditions.

Chapter 6 in Eurocode 3 titled *Ultimate Limit States* governs the design of steel structures under extreme loading conditions. It provides guidelines to ensure structural robustness, safety and reliability at the ultimate limit state - the point where the structures face the most severe loading scenarios without compromising their structural integrity. This chapter also covers the intricacies of member and connection design, load distribution and ductility under extreme loading conditions. This sets the industry standard for crafting steel structures capable of withstanding the most demanding challenges posed by the ultimate limit state, ULS.

The non-dimensional slenderness, $\bar{\lambda}_{LT}$, for a structural member is presented in equation 2.3 where M_{Rd} is the design moment resistance of the member, representing the moment resistance in bending. M_{cr} represents the members critical buckling moment..

$$\bar{\lambda}_{LT} = \sqrt{\frac{M_{Rd}}{M_{cr}}} \quad (2.3)$$

The value to derive the lateral-torsional buckling resistance reduction factor for steel members, ϕ_{LT} , is calculated according to Equation 2.4 where α_{LT} is an imperfection factor and λ_{LT} is the non-dimensional slenderness. To decide on the imperfection factor a table in Eurocode showcasing different types of cross sections is used. For the trusses used in the report the buckling curve d in Eurocode, giving $\alpha_{LT} = 0.76$, is of interest.

$$\phi_{LT} = 0.5 \cdot [1 + \alpha_{LT}(\bar{\lambda}_{LT} - 0.2) + \bar{\lambda}_{LT}^2] \quad (2.4)$$

The lateral-torsional buckling reduction factor, χ_{LT} is calculated according to Eurocode chapter 6.3 in equation 2.5. This is used to adjust the critical buckling resistance of a member calculated under idealised conditions to account for the effects of non-ideal conditions. The reduction factor is multiplied with the critical design moment to obtain the new design value being used. $\bar{\lambda}_{LT}$ represents the slenderness and ϕ_{LT} symbolises the lateral-torsional resistance parameter. A plot of different χ_{LT} depending on α_{LT} is given in Figure 2.1, from where the reduction factor also can be estimated.

$$\chi_{LT} = \frac{1}{\phi_{LT}^2 + \sqrt{\phi_{LT}^2 - \bar{\lambda}_{LT}^2}} \quad (2.5)$$

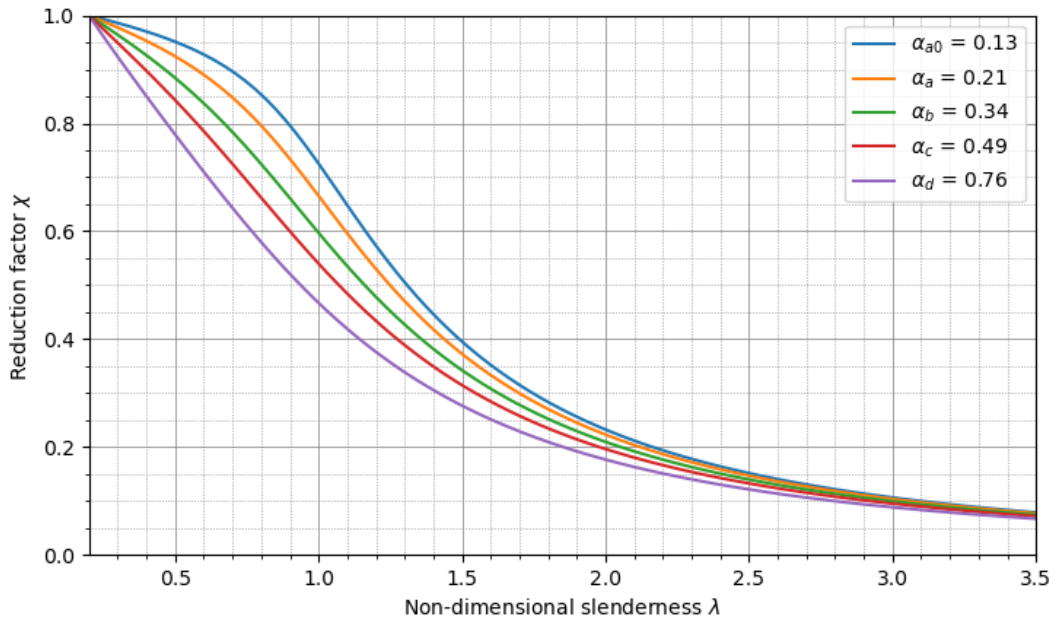


Figure 2.1: Reduction factor as a function of slenderness and imperfection factor.

2.3 Finite Element Method

2.3.1 Overview

The finite element (FE) method can be used in mechanics where traditional analytical methods are not sufficient to solve the complexity of the problem. Its methodology includes dividing a structure into smaller segments, also known as finite elements. A numerical procedure is used with differential equations solved in an approximate manner over every finite element. The elements are assembled to shape the entire geometry. Hence, an approximated solution of the investigated body has been created. [6]

The usage of the method includes multiple problems such as groundwater flow, heat conduction, and elastic behaviour of structures. Depending on the area chosen, the finite element formulation will vary. Further variations are found within the dimension of the problem. Solutions can be made for both scalar and vector field problems. [6]

To simplify the use of the FE method, there are multiple programs where the method is being used for calculations [6]. Abaqus can be found among these, further explained in Chapter 2.4.

2.3.2 Description of the Finite Element Method

As the FE method includes dividing the object of interest into smaller elements, the calculations are done through matrix algebra where a set of equations represent the behaviour of an element. In its simplest form, the element balance equation for one finite element can be described as the following:

$$\mathbf{K}^e \mathbf{a}^e = \mathbf{f}^e \quad (2.6)$$

which for instance in matrix form for a spring can be written

$$\begin{bmatrix} k & -k \\ -k & k \end{bmatrix} \begin{bmatrix} u_1 \\ u_2 \end{bmatrix} = \begin{bmatrix} P_1 \\ P_2 \end{bmatrix} \quad (2.7)$$

where \mathbf{K}^e symbolises the element stiffness matrix, \mathbf{a}^e the nodal displacement vector, and \mathbf{f}^e the element force vector. In Equation 2.7 the k represents the spring stiffness, u_i the displacements in the nodes of the spring, and P_i the force acting at the nodes. Hence, the \mathbf{K}^e -matrix represents the element properties, while the boundary conditions and forces acting on the element determine the known parameters of the \mathbf{a} - and \mathbf{f} -vector. [6]

The properties of each element and its loading are described by their specific matrices and vectors. Thereafter, the properties can be assembled to describe the absolute problem, in the method represented by the global matrix. The global set of equations representing the problem to be solved can then be expressed as

$$\mathbf{K}\mathbf{a} = \mathbf{f} \quad (2.8)$$

The elaborate formulation of the equation depends on the physical phenomenon being studied, and a prominent use of the method includes 2D and 3D elasticity. To calculate the \mathbf{K} -matrix, the element's shape functions are used. In algebraic form, the stiffness matrix for 3D elasticity is written

$$\mathbf{K} = \int_V \mathbf{B}^T \mathbf{D} \mathbf{B} dV \quad (2.9)$$

where \mathbf{B} represents the derivatives of the so-called shape functions. The shape functions are functions used to interpolate the unknown within the element and are sometimes referred to as interpolation functions. The element material properties can be found in the constitutive matrix \mathbf{D} . When performing the calculations, the f -vector is divided into three different parts; \mathbf{f}_b , \mathbf{f}_l , and \mathbf{f}_0 . They represent the boundary vector, the load vector, and the initial strain vector respectively. The formulation of the vectors can be found in equation 2.10-2.12 [6]

$$\mathbf{f}_b = \int_{S_h} \mathbf{N}^T \mathbf{h} dS + \int_{S_g} \mathbf{N}^T \mathbf{t} dS \quad (2.10)$$

$$\mathbf{f}_l = \int_V \mathbf{N}^T \mathbf{b} dV \quad (2.11)$$

$$\mathbf{f}_0 = \int_V \mathbf{B}^T \mathbf{D} \boldsymbol{\varepsilon}_0 dV \quad (2.12)$$

where \mathbf{N} is the shape functions. In equation 2.10, the S_h represents the homogeneous essential boundary conditions, where the constraint has been prescribed to zero in displacement or other kinematics. The given natural boundary conditions are represented by S_g . In equation 2.11, \mathbf{b} refers to the body force vector which accounts for volumetric forces that act throughout the body. Lastly, $\boldsymbol{\varepsilon}_0$ represents the initial strains, e.g. due to thermal expansion. [6]

2.3.3 Nonlinear Analysis

Nonlinear finite element analysis (FEA) involves accounting for both material and geometric nonlinearities that affect the behaviour of the structure. This is in contrast to linear analysis, where it is assumed that materials behave linearly [7]. Nonlinear behaviour also arises if boundary conditions are not constant during loading. This is the case for problems involving contact.

Material nonlinearity occurs when the material deviates from Hooke's law, which describes linear behaviour. Geometric nonlinearity arises when the deformations are

large enough to significantly affect the structure's behaviour. In linear analysis, geometric nonlinearity is ignored by assuming small displacements and strains. However, nonlinear analysis acknowledges large deformations, which introduce geometric stiffness and a dependence of the stiffness matrix on other displacements. Phenomena like large displacements and rotations as well as buckling can then be analysed in the method. [7].

The nonlinear analysis can be solved by using the **Newton-Raphson method**. It performs iterations that are repeated for each load increment until a state of equilibrium is found.

In each load increment, the load level is updated and initially, the displacement is set to that of the previous calculation. With each iteration, the tangent stiffness is calculated. To decide on the accuracy of the iteration a parameter called residual, r , is used. It describes the difference between the internal and external forces. Using the residual, a displacement increment, Δu , can be derived from solving Equation 2.13. [7]

$$K^{(i)} \Delta u = -r(u^{(i)}, P^{n+1}) \quad (2.13)$$

The displacement increment is then added to the estimated displacement of the previous iteration, and the process of calculating the stiffness and residual is started again based on the new displacement. A tolerated residual, r_{tol} , is decided on, thus the iterations continue until $r < r_{tol}$ is fulfilled. The procedure is visualised in Figure 2.2. [7]

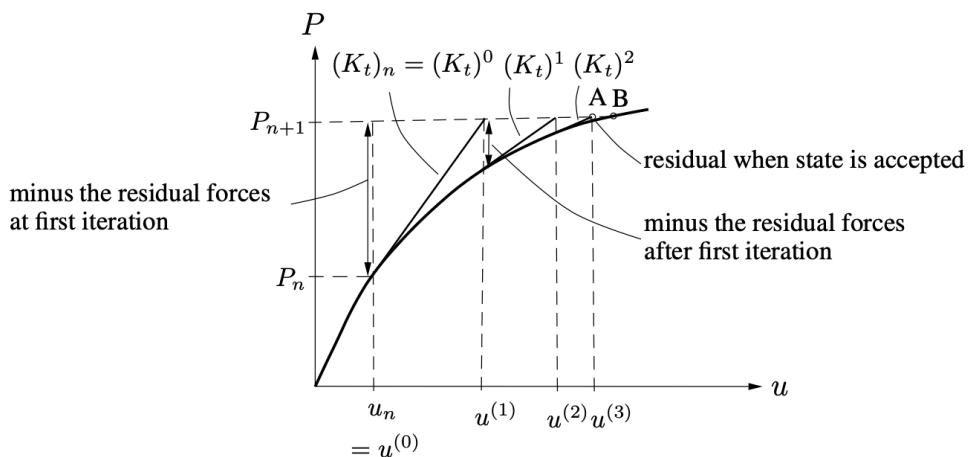


Figure 2.2: Iterations in one load increment that is performed until the residual, r , is in an acceptable state in A, in comparison to the true equilibrium B where $r = 0$. Source: [7].

Sometimes, setting a low r_{tol} can still result in a result deviating far from the true equilibrium. To reduce the risk of an unsatisfactory result, a tolerated displacement increment, u_{tol} , can be established. The iteration process will then continue until both r_{tol} and u_{tol} are satisfactory.

The process of one load step $n = 1 \dots n_{max}$ can be summarised accordingly: [7]

1. Initiate new load level $P = P + \Delta P_n$
2. Start with $u = u_n$
3. Loop while $r < r_{tol}$ and $u < u_{tol}$
 - Calculate the tangent stiffness K_t with u
 - Calculate the displacement increment, Δu
 - Recalculate displacement $u = u + \Delta u$
4. End loop
5. New displacement $u_{n+1} = u$

2.3.4 Analysis Procedures

Buckling analysis refers to a linear elastic structure that is subjected to external loading and experiences proportional deformation, until it reaches a limit where the behaviour is no longer predictable. The deformation that occurs past the limit is called buckling. Due to the geometry and stability of the structure, it will be more or less prone to buckling behaviour [8]. A buckling analysis is a perturbation procedure and can serve as the initial stage in analysing a linear structure or as a subsequent step following preloading, in which case the buckling load is determined as the additional load that can be applied from the preloaded condition. This method is also valuable for assessing the sensitivity of a structure to imperfections. This analysis focuses on the model's response based on its linear elastic stiffness in its base state. It does not consider any nonlinear or inelastic material properties or factors such as time and strain state. [9]

Estimating the buckling behaviour is done by solving an eigenvalue problem. Its formulation is found in Equation 2.14.

$$(\mathbf{K}_0^{NM} + \lambda_i \mathbf{K}_\Delta^{NM}) \mathbf{v}_i^M = 0 \quad (2.14)$$

The stiffness matrix \mathbf{K}_0^{NM} corresponds to the base state including preloads of the structure, while \mathbf{K}_Δ^{NM} represents a geometric stiffness matrix induced by internal axial forces from the external loads due to the incremental loading pattern of the buckling step. Following the base state, eigenvalues are given as λ_i and the mode shapes by v_i^M . Exponents M and N refer to the degrees of freedom of a model, and i to which eigenvalue is being solved. [9]

First order analysis considers linear elastic behaviour with small deflections and assumes that the structure remains in the linear range. Deflections are small compared to the structure's dimensions. It neglects geometric non-linearity. Equilibrium equations are formulated in the undeformed configuration

$$\mathbf{K} = \mathbf{K}_0 \tag{2.15}$$

Second order analysis accounts for non-linearity but assumes small displacements while equilibrium equations are formulated in the deformed configuration. This provides a more accurate prediction for structures under significant loads where linear approximations are inadequate. The stiffness of the structure includes the influence of stress such as the impact of normal force on the lateral stability of columns.

$$\mathbf{K} = \mathbf{K}_0 + \mathbf{K}_\lambda \tag{2.16}$$

Third order analyses also includes additional effects due to large displacements.

$$\mathbf{K} = \mathbf{K}_0 + \mathbf{K}_\lambda + \mathbf{K}_\sigma \tag{2.17}$$

2.3.5 Modelling Elements

Typically, the elements used in FEA are divided into 1D, 2D and 3D based on the elements' shape. Depending on the selection of elements and their dimension, different finite element geometries can be chosen. Selection can be made in terms of geometry and node quantity. Some examples of finite element geometries are given in Figure 2.3. [10]

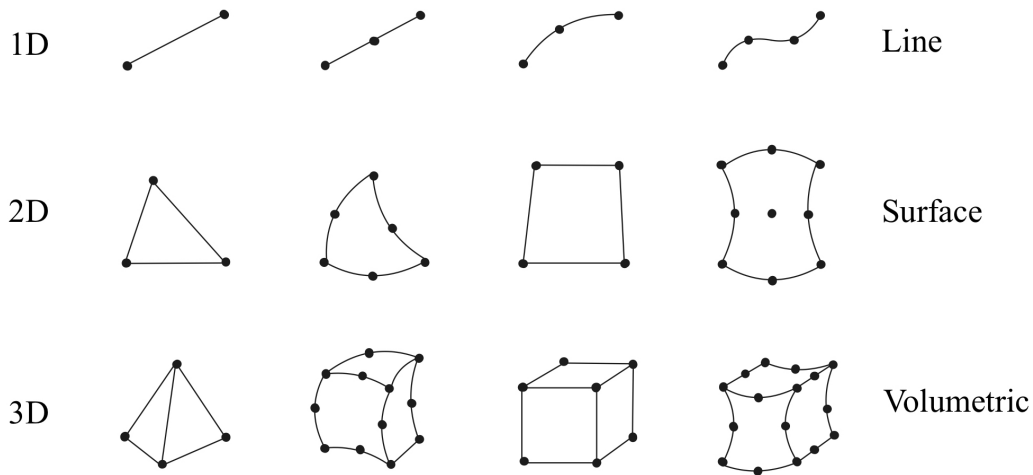


Figure 2.3: Examples of finite element geometries in different dimensions. Adapted from Wai et al. [10]

To perform an analysis, three different element types are often used for the modelling in the respective dimensions: beam, shell, and solid elements.

Beam elements represent one-dimensional line segments within three-dimensional space or confined in the X-Y plane, possessing attributes linked to deformation along the line, which acts like the beam's axis. These deformations include axial stretching,

bending, and torsion (in three-dimensional settings). Beam elements provide flexibility by accounting for transverse shear deformation between the beam's axis and its cross-sectional directions. The advantages of beam elements lie in their geometric simplicity and limited degrees of freedom which saves computational resources during simulations. The simplicity is achieved by assuming that the member's deformation can be approximated only by variables dependent on the position along the beam's axis. Therefore, it is crucial to take into consideration if such simplified one-dimensional elements are appropriate to include in a model when executing simulations [9]. A visual representation of a beam element is presented in Figure 2.4.

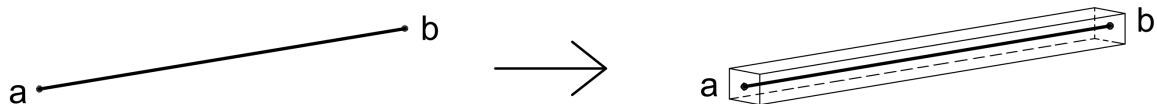


Figure 2.4: Beam Element between endpoints a and b, where the model is shown to the left and its representation to the right.

Shell elements are, in structural mechanics, finite elements used in models of thin-walled structures and plates. These elements are used in FE-analysis to simulate the behaviour of structures subjected to various loads, such as bending, shear and membrane forces. Shell elements are characterised by their ability to represent the geometric and material properties of thin structures efficiently. Unlike solid elements, which model the entire volume of the structure, shell elements are typically used to represent the middle surface of thin structures.

Shell elements have several advantages. By representing the structure with a surface, computational resources are conserved while still capturing the structural behaviour accurately. Thus, shell elements provide accurate results with a coarser mesh compared to solid elements which require a higher mesh density. This also reduces the effort required for meshing, pre-processing and post-processing of FE method models. [11]

Shell elements are employed for modelling structures where one dimension, typically the thickness, is notably smaller than the other dimensions. Utilising this characteristic, conventional shell elements approximate a body by specifying its geometry at a reference surface, with the thickness determined via section property definition. Conventional shell elements are equipped with both displacements and rotational degrees of freedom.

On the other hand, continuum shell elements approximate an entire three-dimensional body where the thickness derives from the element's nodal geometry. Unlike conventional shell elements, they possess only displacement degrees of freedom. Despite their appearance resembling three-dimensional solids in modelling, their behaviour aligns closely with that of conventional shell elements. [9]

Figure 2.5 illustrates the use of conventional shell elements. Herein, conventional shell elements have been used in the modelling since the building components of the truss have cross-sections with a relatively small thickness.

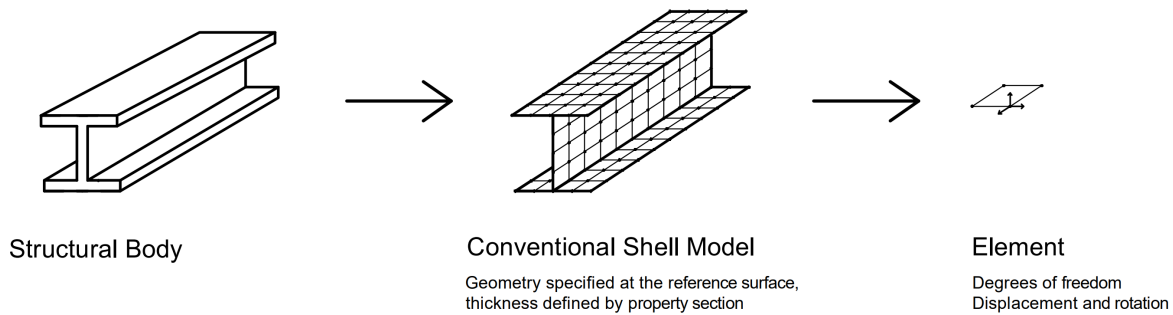


Figure 2.5: Conventional shell element.

Solid elements allows any realistically composed geometry. It's beneficially used for more complex models where line or shell elements are not sufficient since unlike the other element types, the entire geometry is defined in 3D, see Figure 2.6. Each node in the model consists of three degrees of freedom. Although a solid element could technically be used to model all finite element problems, it's not always the most suitable option. It demands far more computational resources considering its more elaborately created geometry and mesh. Therefore, a structure should be modelled as a line or shell element if simplification is possible. [12]

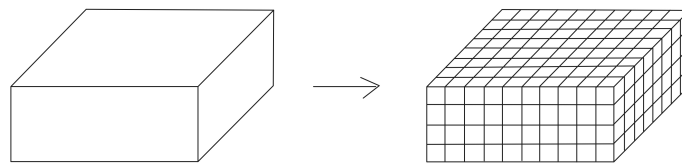


Figure 2.6: Solids define the full geometry in 3D.

2.4 Abaqus FEA

2.4.1 Overview

Abaqus is a powerful finite element analysis software. It's used within a range of industries thanks to its few limitations in modelling. Any physically legitimate combination can be created in terms of elements, loading, and material. Moreover, the software offers a variety of simulations which makes it useful for different problems solved by finite element analysis. These include for instance stress analysis, heat transfer, and mass diffusion. [13]

The modelling in Abaqus is divided into so-called modules, which are functional units with different tools to create the model. These are labelled:

- Part. Creates individual instances by drawing or importing geometry.
- Property. Defines section and material definitions to be assigned to Parts, or sub-volumes of a Part.

- Assembly. Assembles the instances created in Part.
- Step. Creates the steps of the analysis along with outputs.
- Interaction. Specifies the interaction between Parts of the assembled model.
- Load. Defines the loads and boundary conditions in the model.
- Mesh. Creates a finite element mesh.

The modules enable multiple ways of creating a model. Some have a larger impact on the final results of the simulations. For instance, a choice between the models described in Chapter 2.3.5 can be made when creating an instance in Part and its elements in the Mesh module. [9]

2.4.2 Part

In the Part module, instances can either be created or imported into the program. Various parts can be created, such as different types of rigid or deformable. A feature type can be chosen, among those are beam, shell and solids described in Chapter 2.3.5. [9]

2.4.3 Property

The property module is a crucial component used for defining relevant characteristics of the elements used in finite element simulations. Users can define material properties such as Young's modulus, Poisson's ratio, density, thermal conductivity, and elasticity for accurate material behaviour simulation.

This module enables the definition of section properties for various types of structural elements (e.g. truss, beams, shell solid) ensuring compatibility between element behaviour and specified material properties. For shell elements, the simulated thickness is defined in section properties, where the reference surface can be the top, bottom, or middle surface of the element, see Figure 2.7. [9]

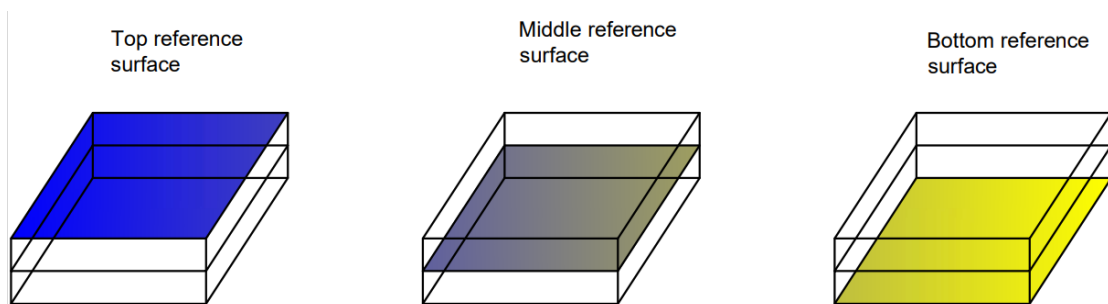


Figure 2.7: Thickness definition from reference surface for shell elements.

2.4.4 Assembly

When creating an instance in Part, it only exists in its local coordinate system. Through the assembly, the instances are placed in a global coordinate system in which they can be aligned to create a larger model. They are still considered separate parts that can be edited and when meshing, the program will create a separate mesh for every instance. To enable interactions between instances it has to be defined in the Interaction module. Otherwise, the parts work as fully independent structures. [9]

A function called **merge** can be used in the assembly. If the model contains instances from multiple parts, the merge function can be used to combine those instances into one part, thus avoiding the need to define complex and time consuming interactions between the parts. With the merge function the intersecting parts, for instance surfaces when using shell elements, will be considered as one part. The boundaries of the intersecting parts can either be retained or removed according to Figure 2.8. [9]

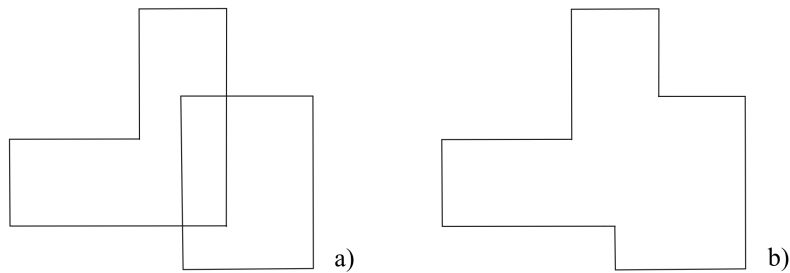


Figure 2.8: Retaining the intersecting boundaries in a) and removing them in b) when merging an assembly.

Merging the parts also avoids having to assign material properties individually to each part, which could be an advantage if many parts carry the same properties. On the other hand, merging could restrict property definition since intersecting regions have been combined. For instance, two beams with different material properties that share a surface can no longer be assigned properties separately. [9]

2.4.5 Step

The step module defines which type of analysis is performed. They can be performed through two different procedure types: **General** and **Linear perturbation**, where the procedure General is used for nonlinear analysis steps and with the sub-option of accounting for large displacements. [9]

A **General** step can contain material, geometric, and boundary nonlinearity, but can also be used for linear problems. To solve the nonlinear equations, the Newton-Raphson method is used. Hence within the General step, the incremental loading and iteration scheme of Figure 2.2 is used. Each step has a specific time set which begins at zero for every step. It allows for setting a physical time scale when performing for instance a dynamic analysis, and can otherwise be set to an arbitrary time. [9]

The **Linear perturbation** type can be appropriate if the system can be approximated as linear. Unlike General steps, the linear perturbation analysis does not utilise an incremental loading approach and does not influence subsequent analysis. If no previous analysis has been performed, the initial conditions will be used. Given that the previous Linear perturbation steps are never utilised, they can advantageously be used in between General steps without affecting the following General step. Furthermore, the step type has no time period. [9]

The procedures used in the dissertation are **Static** and **Buckle**. Static was used with both General and linear perturbation procedure types while Buckling is Linear perturbation.

A **Static** analysis calculates the response of the system due to different static loads. It utilises the material definition along with boundary and load conditions to solve the finite element balance equation of the global system.

The analysis can be used when inertia or time-dependent material effects do not have to be taken into account. It can solve problems of both linear and nonlinear behaviour. When solving a nonlinear equilibrium Abaqus uses Newton's method, which gives a result in the form of a series of increments. [9]

The **Buckling** procedure performs an eigenvalue buckling prediction. It can be used to estimate the critical load of structures and investigate the imperfection sensitivity.

When performing the analysis, results will be given by showcasing mode shapes and a corresponding eigenvalue. Estimation of the eigenvalues is done using Equation 2.14. The amount of eigenvalues requested can be done in the step settings. Moreover, the type of eigensolver is chosen between Lanczos and Subspace. Their efficiency varies with the number of eigenvalues requested, Lanczos is typically faster but Subspace can be quicker with less than 20 eigenmodes calculated. The Lanczos solver has some restrictions, for instance it cannot be used with a model containing coupling constraints. [9]

2.4.6 Interaction

Interactions between separate instances in one assembly are defined in the interaction module. A substantial amount of functions can be utilised to create connections and dependability in the program. Four versions were mainly used, described in the chapter.

The surface-based **Tie** constraint links two surfaces throughout a simulation, exclusively within surface-based constraint frameworks. It is applicable in mechanical displacement simulations and can be employed to synchronise a surface's motion with that of a three-dimensional beam. This has the benefit of aiding mesh refinement, particularly in three-dimensional problems. This constraint ensures that nodes on the slave surface mimic the motion and properties of the closest point on the master surface. Additionally, it automatically considers the initial thickness and offset of underlying shell elements. The constraint optimises computational efficiency in bigger

models by reducing degrees of freedom for constrained slave surface nodes wherever capable. Abaqus does not constrain slave nodes to the master surface unless they are included in the tied node set or within the tolerance distance from the master surface. Any slave nodes not satisfying this criterion will remain unconstrained for the duration of the simulation and will never interact with the master surface as part of the tie constraint. The Tie constraint is therefore useful to simulate a strong welding between parts in certain areas, see Figure 2.9. Systèmes [9]

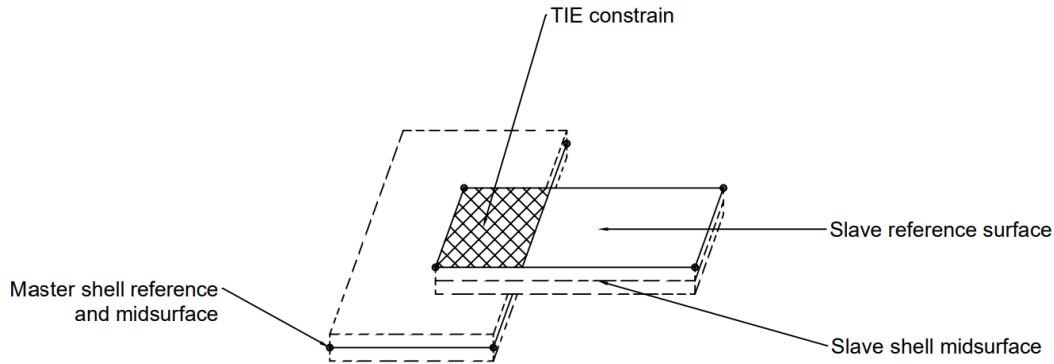


Figure 2.9: Tie constrain between two parts.

Multi-point constraints (MPCs) allow constraints to be improvised between different degrees of freedom of the model and can be quite general. The type of constraint was used between different parts of the truss beam analysed. The constraint corresponds to the presence of a rigid beam between two nodes, to constrain the displacement and rotation at the first node to the displacement and rotation at the second node, see Figure 2.10. [9]

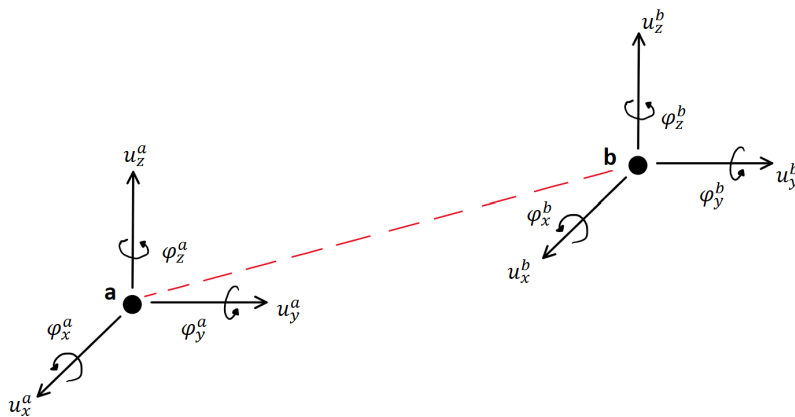


Figure 2.10: MPC type BEAM between nodes a and b.

The surface-based **Kinematic coupling constraint** links the movement of a set of nodes on a surface to a designated reference node. The constrained nodes are tied to a rigid body motion determined by the reference node, see figure 2.11. It can be applied with stress/displacement elements and can be utilised in both geometrically linear and nonlinear analyses. The coupling constraint is useful for simulating end conditions such as a rigid cross section which is assumed to not deform. It is also a practical tool for when load distribution follows a moment-of-inertia expression which

is evident in scenarios like classic bolt-pattern. Coupling facilitates modelling by making interactions with other constraints possible, such as connector elements, which enhances the versatility of the modelling approach. [9]

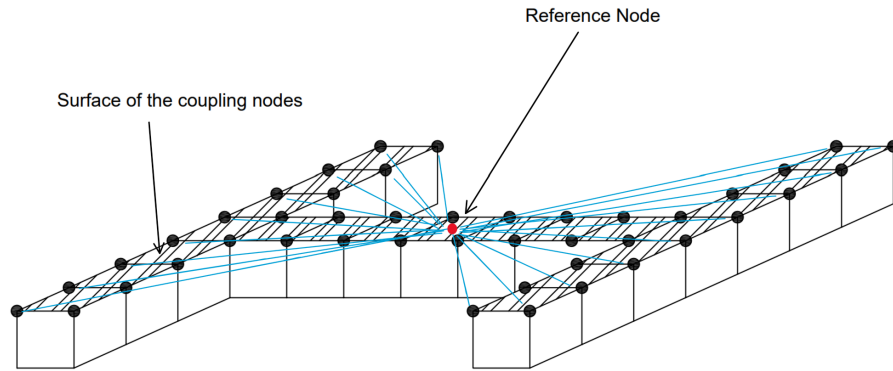


Figure 2.11: Kinematic Coupling Constraint.

The **Connector elements** constraint makes the global displacements and rotations of two nodes dependent on each other by introducing linear or nonlinear behaviour in terms of springs and other components, see Figure 2.12.

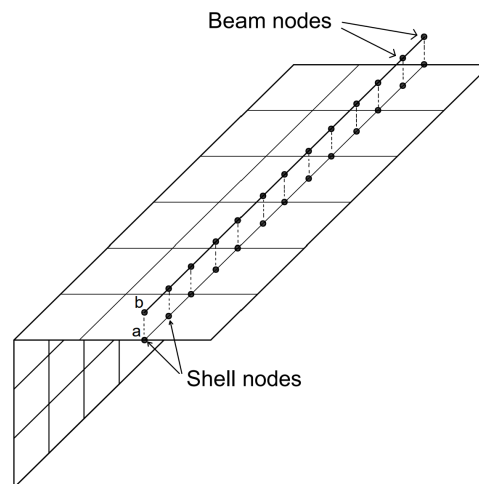


Figure 2.12: MPC type BEAM.

2.4.7 Load

As the name implies, the Load module contains the load conditions of the model along with boundary conditions. The load and boundary conditions can be varied with different steps or remain continuous during the full simulation. [9]

2.4.8 Mesh

Mesh attributes are defined and generated in the Mesh module. Selections can be made in terms of mesh geometry, density, technique, etc. Likewise as Figure 2.3, the dimension of the element will determine the possibilities of mesh attributes. [9]

Mesh Convergence Study

Mesh convergence studies are crucial in finite element analysis to ensure accurate and reliable simulations. Engineers can determine the minimum mesh density by progressively refining the mesh and observing how the results converge. This ensures that the simulation results are accurate enough. Mesh convergence studies also aid in optimising computational resources by identifying the optimal mesh density required to achieve convergence. During the study, mesh-related errors were found and fixed improving the overall quality of the simulations.

3 Modelling Approaches

3.1 Method

3.1.1 Simplified Model

Initially, a simplified model of a simple arbitrary steel truss was created. In Chapter 4 a specific truss from MAKU AB will be investigated, hence the simple model was created as a version containing some properties of the MAKU truss. The purpose was to investigate how to efficiently and thoroughly model using Abaqus, before using the complex building of interest. An as simple modelling technique as possible was sought, without significantly impacting the result regarding deflection and buckling. The trials were narrowed down to four different ways of modelling the structure. They can briefly be described as:

- A. Using shell elements for the top and bottom chords while the diagonals are modelled using wires, connecting the parts using constraints.
- B. Using shell elements for all parts of the truss and assembling them through an automatic merge procedure, resulting in one truss being treated as one part.
- C. Using shell elements for all parts of the truss and assembling them through constraints, resulting in one truss consisting of several parts that are connected.
- D. Combining B and C by using shell elements for all members and assembling groups of parts by merging them, and assembling the groups through constraints.

The truss was created using three frames of three meters each with a few decimetres addition on the edges, giving the top beam a length of 9.5 and the bottom of 6.5 meters. Its height was set to 1.5 meters, giving angles of 45 degrees for the diagonals of the truss. A simple illustration of the truss with its measurements can be found in Figure 3.1.

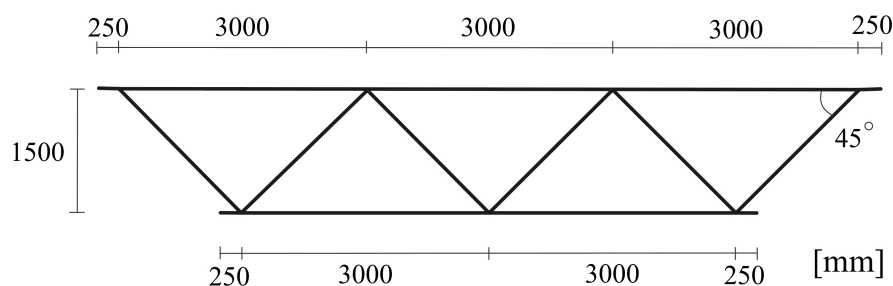


Figure 3.1: Simplified truss used for initial modelling in Abaqus.

3.1.2 Property Definition

As the truss represents a simple version of the one from MAKU, the beam properties according to company specifications were used. The properties were kept equal in all trials to ensure the comparison depending on the modelling technique while disregarding external factors. Structural steel type S355 was used in all components of the structure and therefore the density, ρ , of the material was 7850 kg/m³. The modulus of elasticity, E , was of 210 GPa and Poisson's ratio, ν , of 0.3.

Similarly to the MAKU truss, two L-beams each were used to create the top and bottom chords. As for the diagonals, UPE 120 was used. Specifications of the sections can be found in Table 3.1 and section drawings in Figure 3.2.

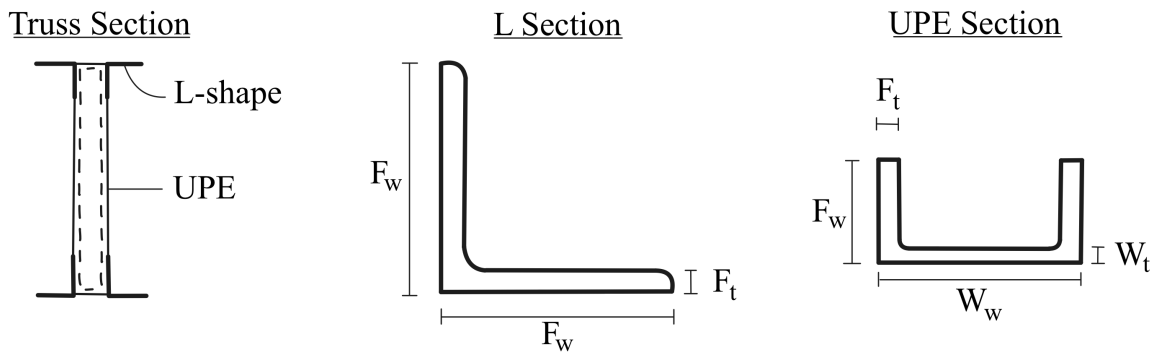


Figure 3.2: Section of truss and the two section types.

Table 3.1: Dimensions of sections used in the truss.

Section type	Flange w	Web w	Flange t	Web t
L 150	150 mm	-	15 mm	-
UPE 120	60 mm	120 mm	8 mm	5 mm

When assigning a section in Abaqus, different settings can be used when defining the thickness of the shell. A specific side of the shell can be chosen to project the thickness, meaning that the shell acts as one side of the section as seen in Figure 3.3. Also seen in the figure, another option relevant to modelling the objective is using the shell as the middle section, projecting the thickness on both sides.

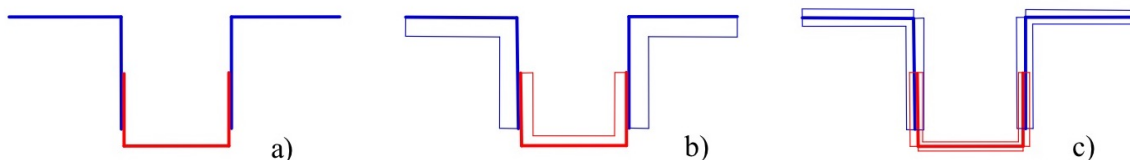


Figure 3.3: Different ways of defining the thickness of the shells. Figure a is a section of the top L-beams and one UPE beam, figure b shows the thickness defined on one side of the shell, while figure c shows it defined with the shell in the middle section.

Figure 3.3 showcases that defining the thickness on one side gives a model that closer resembles the structure of the MAKU truss. However, when assembling the truss system using approach B in Abaqus, the merged assembly was automatically placed with the shell as the middle section. As multiple elements intersect, specifically where the UPE beams are connected to the L beams, the intersecting parts cannot be given separate property values as those are now regarded as one part. Hence, approach B is best performed using the middle surface. To make the comparison as accurate as possible, the middle surface option was used for all models.

3.1.3 Load and Boundary conditions

To enable a valid comparison between different methods, similar load and boundary conditions were used. An arbitrary load of 1 kN/m^2 , giving 0.3 kN/m with a flange width of 0.3 m , and direction downwards was placed on top of both L-flanges. A visualisation of the load can be found in Figure 3.4 where the placement of the load is shown from two directions.

Boundary conditions were applied at the ends of the L-beam on both sides. On one side, it was defined as pinned. The other side was defined as roller support, allowing displacement in the beam's direction, see Figure 3.4.

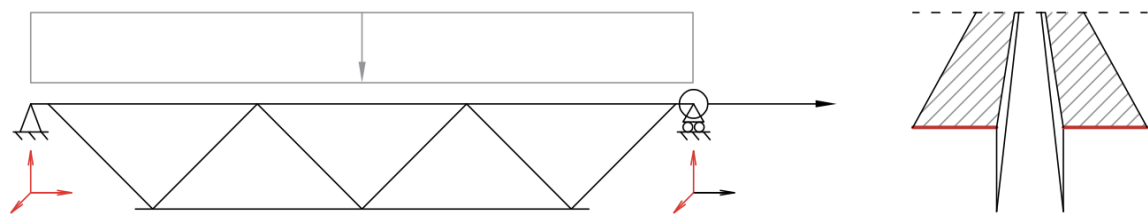


Figure 3.4: Boundary conditions and load of the truss are given with prescribed displacement in red and load in grey. The section view shows how the load is placed on the striped surfaces of the L flanges and boundary conditions applied on the red edge.

3.1.4 Step and mesh

Since deflection was to be investigated in the larger model, it was used for comparison between the trials. It was seen as an appropriate measurement for comparison by calculation through a linear analysis. Buckling on the other hand, given its nonlinear behaviour, was not used for reference although it would be investigated in the larger model. To model the deflection when comparing the models as simple as possible the Static Linear perturbation step was utilised.

A fairly dense mesh of 10 mm element size was used in when comparing the models. It was deemed dense enough to not impact the result substantially while, due to the model being relatively small, still acquiring fast simulation time.

3.1.5 Model A

Model A can be described as the most simple one of the three. While the top and bottom beams consisted of shell elements, diagonals were modelled using a wire. In total, the model consisted of five different parts, see Figure 3.5.

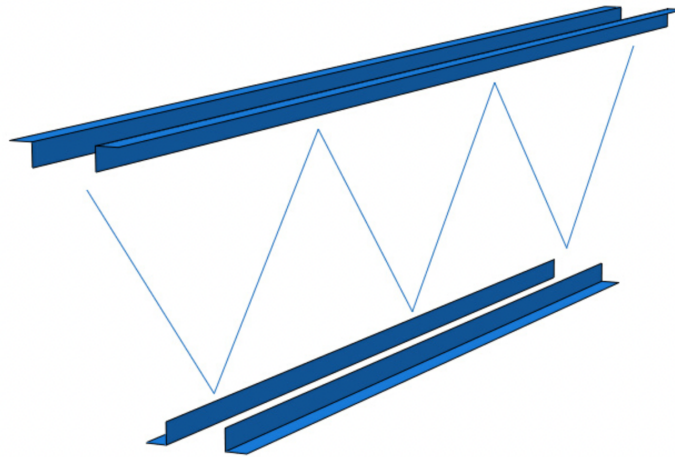


Figure 3.5: Exploded view of parts when using a shell for top and bottom beams but a wire for the diagonals

The shape of the sections in the shell elements was drawn in the Part module mentioned in Chapter 2.4.2, with only material properties and thickness being assigned to the parts. When using wire, on the other hand, lines were used to represent all diagonals. These lines could in turn be given all properties in the property definition, including the section. The method allows for faster assembly regardless of the truss's length, since all diagonals are one part. It also enables the thickness of the parts to be assigned more realistically by using the method shown in Figure 3.3b, although the method of 3.3c was used in the trial for comparison.

When creating the interaction between the parts, a rigid constraint was used where the nodes of the tops and bottoms of the zigzag pattern representing the UPE beams were tied to the inner side of the L beams. It allowed for the distance between the L beams to still be the width of the UPE beams, with the diagonals placed in the middle of the gap. The nodes of the diagonals were defined as masters and the L beams were defined as slaves. Consequently, the connecting node of the top and bottom chords will be rigidly connected to the diagonals.

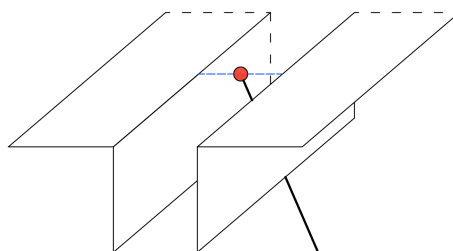


Figure 3.6: Connection between top node of diagonal, red, to L chords drawn in blue.

3.1.6 Model B

In model B, shell elements were used for all parts. When creating the interaction between the parts to establish the welded connections of the truss, an automatic merging procedure was used as described in Chapter 2.4.4. This created one large part containing the entire truss, see Figure 3.7.

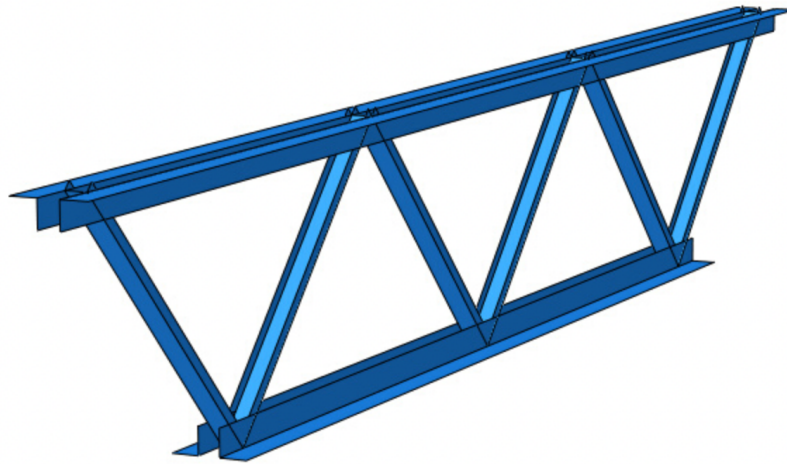


Figure 3.7: Part when modelling through merging all components.

Through the merge, all parts of the beams that coincided were turned into one surface. Consequently, it affected the thickness of those coinciding areas. While previously consisting of both the L and UPE beams with their corresponding thickness, some surfaces had to separately be assigned the sum of both thicknesses. It had to be performed manually after the merging procedure.

3.1.7 Model C

The most elaborate model was C. Shell elements were used for all parts without merging, creating the largest number of parts as seen in Figure 3.8.

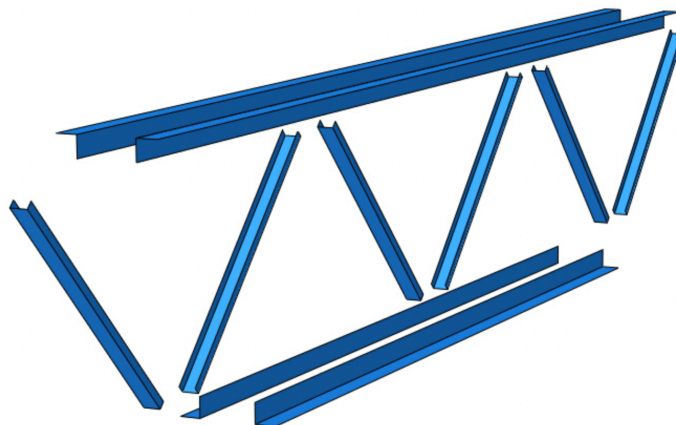


Figure 3.8: Exploded view of parts when keeping the flanges and diagonals separate and intersecting them using constraints.

The welding of the truss was created in a similar way as model A, where constraints consisting of a rigid tie were used. In the model, the L flanges were defined as masters, and UPE flanges as slaves.

Using model C also allows for using the adjusted placement of the thickness according to Figure 3.3, but as in model A the middle surface option was used for comparison purposes.

3.1.8 Model D

Model D was defined as a combined version of B and C, where both the merge function and constraints were used. The top flanges were merged into one part, the bottom flanges into one, and lastly diagonals as one part, see Figure 3.9.

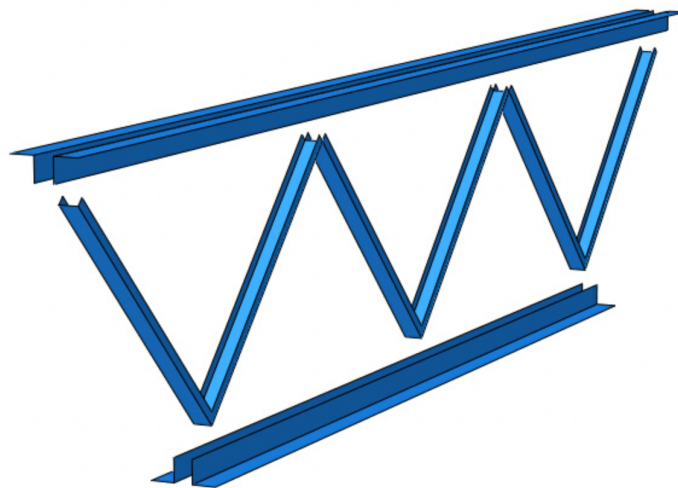


Figure 3.9: Exploded view of parts when merging the top flanges, bottom flanges, and middle section separately and intersecting them using constraints.

Since the UPE beams and L beams were separate parts, the issue regarding coinciding parts with different section properties in model B could be avoided. It allows for assigning the thickness on either side of the shell as displayed in Figure 3.3b. However, the method was less detailed than model C, since parts of the UPE beams were still merged, but consisted of fewer parts and constraints which would allow for a possibly faster assembly.

3.1.9 Mesh Convergence Analysis

A mesh convergence analysis was conducted to find the most ideal mesh size. The target was to find an element size which is as large as possible, due to a shorter simulation time, while still not affecting the result substantially. It's most importantly a guideline on which element size to use when investigating the larger model in Part 2. Hence, the steps chosen in the investigation were Static General and Buckling since these were to be used in Part 2. In the Buckling step, 10 eigenvalues were requested.

The analyses were made on models as described above. A starting element size of 100 mm was used. The size was then lowered until only a minor difference in the results in terms of deflection and eigenvalue could be found.

3.2 Results

3.2.1 Deflections

As a result of the load placement and lack of a stabilising roof attached to the top flanges, the largest deflection in all computations could be found locally on those flanges. However, the global deflection of the truss is of interest. A node on the intersection between the UPE beams in the middle of the bottom beam was chosen, in the tables referred to as u_{mid} . The maximum deflection of the structure is given as u_{max} . Moreover, a percentage difference is presented between the u_{mid} .

Initially, the effects of the property definition regarding thickness placement were investigated. Since model C was deemed to be the most thorough model it was used for the comparison. Two different trials were made, one where the shell was defined as one of the outer surfaces and one where the shell was defined as the middle surface according to options b and c in Figure 3.3. A percentage comparison was also made, with the second option as a reference. The result is presented in Table 3.2.

Table 3.2: Deflection when testing the placement of the thicknesses according to Figure 3.3, using model C for the trials.

Trial	u_{max} (mm)	u_{mid} (mm)	%
Thickness Option b)	0.207	0.0893	93.5%
Thickness Option c)	0.211	0.0955	Reference

According to the result, there is a substantial difference between the definition of thickness. Given the small deflection in the investigated case, with a rather short truss and small load, the difference in millimetres is minor. However, the percentage difference is greater.

Thereafter, a comparison between the models was made regarding deflection, presented in Table 3.3. Model A differs from the others with a decreased deflection of approximately 25% compared to model C. This is the result of using different element types in the same model, where connections between the types lead to an inaccurate representation of how the truss behaves under load impact. It is noteworthy that models C and D obtained the same deflection values which indicates that merging parts with equal properties does not affect the results according to this specific model.

Table 3.3: Deflection in the different models.

Trial	u_{\max} (mm)	u_{mid} (mm)	%
Model A	0.179	0.0663	74.3%
Model B	0.209	0.0889	99.7%
Model C	0.207	0.0893	Reference
Model D	0.207	0.0893	100%

3.2.2 Choice of model

Since the MAKU truss was to be investigated using multiple different and larger models, a trade-off on assembling the truss regarding time efficiency was also made. In terms of creating only one truss, the time consumption was fairly similar between the models. Although, in terms of creating more trusses for a building the time would vary largely.

Model B would be the most time-efficient one when assembling multiple trusses. Creating one truss was fairly complex as the property definition demanded more work than the other models, but assembling multiple trusses would more than compensate since only one part has to be used for each truss. Moreover, no constraints have to be defined within the truss which saves more time as more trusses are used.

The most time-consuming when using multiple trusses would be to use model C. Although it was fairly simple to assemble into one truss, in contrast to model B the time taken to assemble would exponentially increase with more trusses as the constraints have to be defined internally on every truss. Given its large amount of parts, which would be even more on the larger MAKU truss, it's an inefficient way of modelling.

Model A and model D were fairly similar in efficiency. Although model A was faster when creating one model, they both entail the same amount of parts, three each, for every truss being created. Moreover, they demand approximately the same amount of constraints internally. Both models are a faster way of modelling compared to model C, although they are significantly more time-consuming than B.

Given the results when comparing deflections, no difference was found between models C and D. This indicates that the simplifications made in model D had no significant impact on the model created. Model A deviated largely from the other models in terms of deflection and was therefore immediately eliminated as an option.

When comparing the models' deflections, model B showed a minor difference. However, the difference in thickness definition reflects negatively on model B given its inability to define it any other way than the shell as the middle surface. The combination of the deflection difference in the model and thickness comparison entailed that model B was discarded as an approach.

In conclusion, model D was chosen as a modelling technique in the computations. It

gave equal results as the most thorough model but was significantly more time-efficient in larger constructions.

3.2.3 Mesh Element Size

Similar to the model comparison, a specific point in the intersection at the bottom of the middle diagonals was chosen to evaluate deflection. The same point was used in all comparisons for a consistent comparison.

In terms of buckling, the first global mode shape was used for comparison. If local buckling appeared before, these were neglected.

Table 3.4: Trials of Model D with different element sizes.

Global Element Size (mm)	Deflection (mm)	Difference (mm)	1st Eigenvalue (kN/m)	Difference (kN/m)
100	-0.8389	-	Only Local	-
90	-0.5281	0.3108	86.88	-
80	-0.5326	-0.0045	70.26	-16.62
70	-0.5344	-0.0018	69.75	-0.51
60	-0.5114	0.023	74.46	4.71
50	-0.5122	-0.0008	73.89	-0.57
40	-0.5049	0.0073	74.04	0.15
30	-0.5030	0.0019	74.61	0.57
20	-0.5010	0.0020	74.40	-0.21
10	-0.5000	0.0010	74.58	0.18
7.5	0.5000	0.0000	74.52	-0.06
5	-0.4998	0.0002	74.49	-0.03

As seen in Table 3.4 the largest element size could not produce a global mode within the 10 requested eigenvalues. When looking at the difference in both deflection and eigenvalue the result seems to converge at an element size of 30 mm. Moreover, the eigenvalue seems to stabilise between 74 – 75 kN/m.

Although the differences in deflection and eigenvalue are rather small between most mesh sizes, the difference can have a greater impact on the larger model. The chosen mesh size for the larger model was therefore 30 mm.

4 Analysis of an Industrial Building

4.1 Description of Industrial Building

4.1.1 Components

An industrial building composed of a corrugated steel roof, trusses spanning along the roof, and columns carrying the trusses were analysed. A few different versions of the building were tested, one can be seen in Figure 4.1.

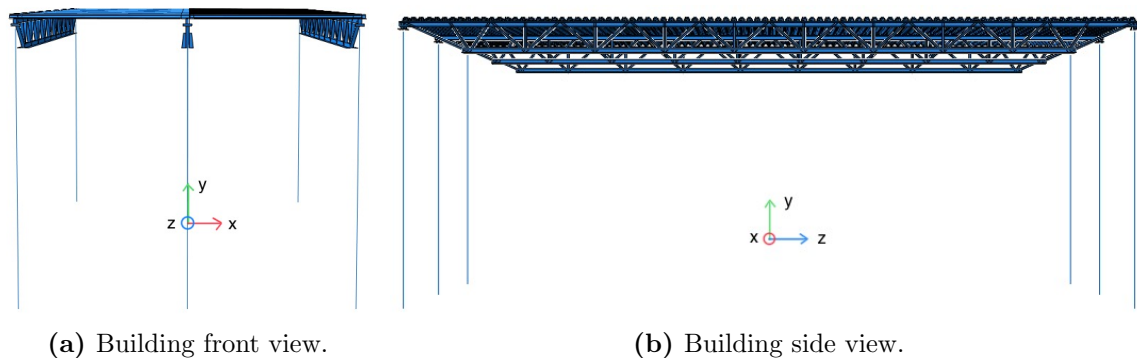


Figure 4.1: Building tested

To simulate a realistic scenario, the components were taken from manufacturers' product catalogues. The corrugated steel roof was modelled according to the producer Ruukki's load-bearing sheet T153-40L-840, details are specified in Appendix B. Furthermore, a steel truss from manufacturer MAKU Stål AB was used for modelling. The dimensions of the parallel truss were decided using their sizing guide and recommendation from AFRY. The selected truss was a parallel truss named U 150-150-120-1100, which had a length of 26.4 meters, a height of 1.1 meters and contained 10 sections, see geometry in Figure 4.2.

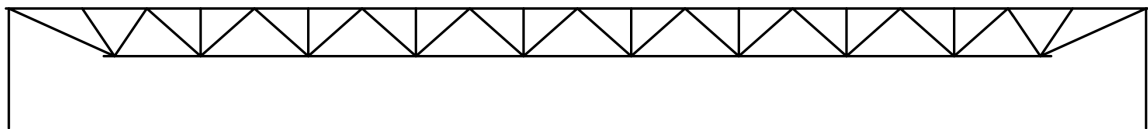


Figure 4.2: Structure of the selected truss.

The dimensions for half of the truss are presented in Figure 4.3. Since the truss has a symmetrical shape the dimensions are implemented for both sides. The MAKU trusses consist of two L-beams for each of the top and bottom chords. All diagonal beams are UPE beams. However, the beam type of the vertical elements remained unclear in the detailed description. Thus, these were also assumed to be of the same type as the diagonal parts. A section drawing can also be found in Figure 4.4.

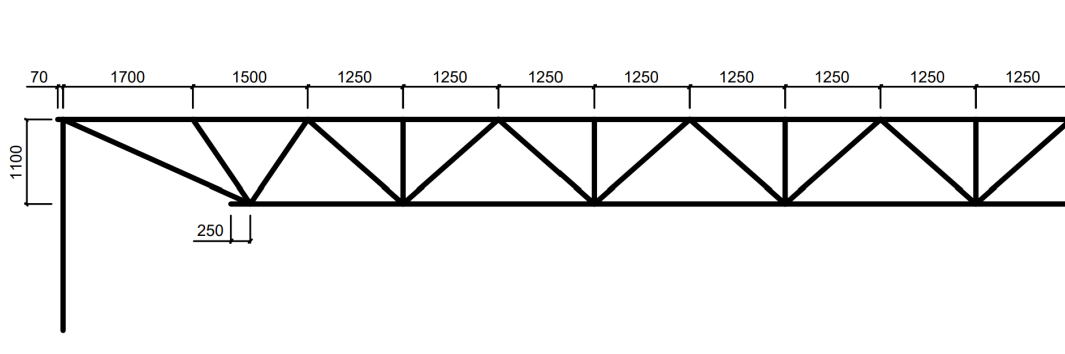


Figure 4.3: Measurements of the truss.

According to the available detail drawings from MAKU, see Appendix A, all UPE beams are oriented with the open side toward the roof. Again, little information was found regarding the vertical elements, hence these were assumed to be oriented towards the centre of the truss.

The attachment of the truss to the columns consists of one short HEB (4) placed inside a horizontal UPE (3) which is bolted to the underlying construction (5), see Figure 4.4. Due to a lack of information from MAKU regarding the attachment to the columns, as the only information available can be seen in Appendix A, an assumption was made about the connection. Based on information regarding similar constructions from AFRY, the attachment was modelled with a thick steel plate of 25-30 mm connected with bolts from the UPE beams, which in turn were welded to the HEB columns. A detailed drawing of the connection can be seen in Figure 4.4, with numbers representing the entities in Table 4.1.

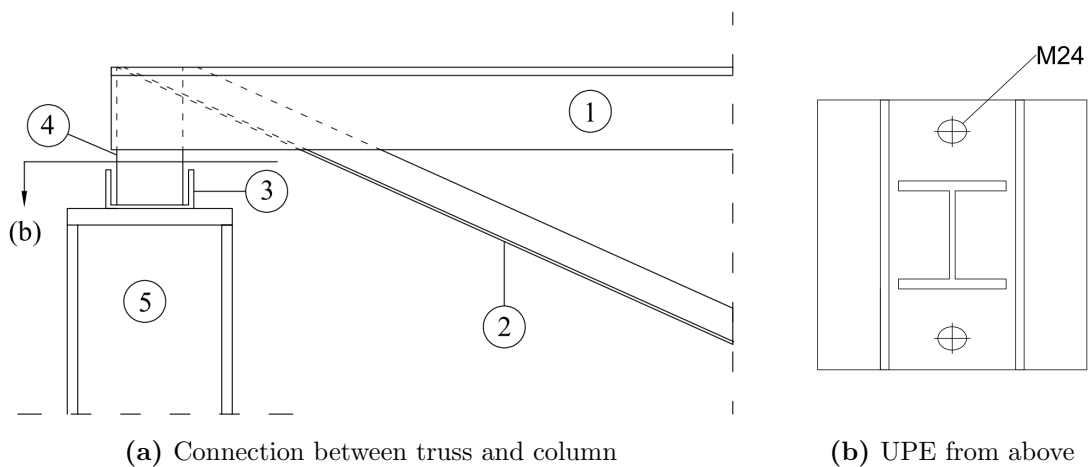


Figure 4.4: Details of connection between truss and columns.

4.1.2 Dimensions

Dimensions of the truss were decided on using the specifications from MAKU Stål AB. The column section and size were based on the one modelled by Tosovic [1], as the analysis is conducted on the same building. All dimensions of beams used in the model are presented in Table 4.1. The thick plate used in the column connection was set to 30 mm in calculations.

Table 4.1: Dimensions of sections used in the truss and columns.

Nr.	Section type	Flange w	Web w	Flange t	Web t
1	L 150	150 mm	-	15 mm	-
2	UPE 120	60 mm	120 mm	8 mm	5 mm
3	UPE 160	70 mm	160 mm	9.5 mm	5.5 mm
4	HEB 120	120 mm	98 mm	11 mm	6.5 mm
5	HEB 300	300 mm	262 mm	19 mm	11 mm

The CGI Roof was modelled according to profile drawings taken from the manufacturer Ruukki with a pitch of 280 mm, the distance between two crests, see Figure 4.5. The thickness of the roof varies between 0.7-1.5 mm according to Ruukki's product specification. Based on previous research by Tosovic [1], the thickness of the roof was set to 0.8 mm.

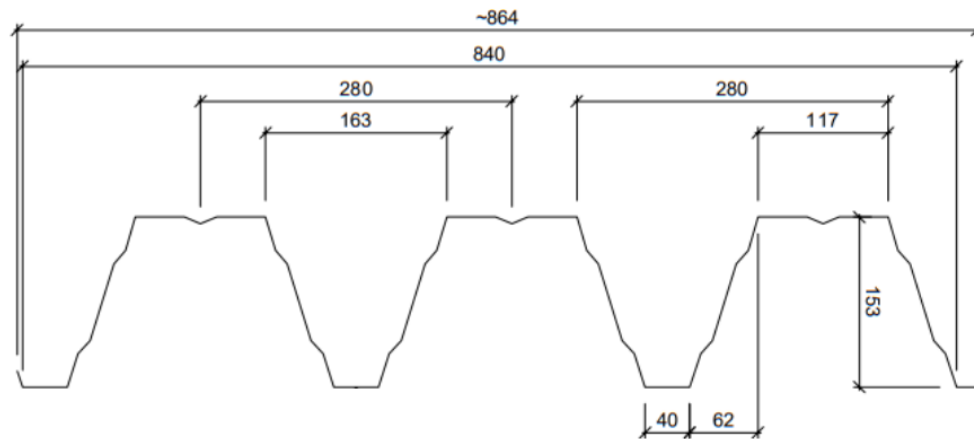


Figure 4.5: Profile drawing of CGI plates roof used in the model. From manufacturer Ruuki.

4.2 Abaqus Model

The model in Abaqus was created using shell elements for all parts except the HEB 300 columns, for which beam elements were used. The members modelled with shell elements had a defined thickness according to details from the manufacturer and were assumed to be welded together where no connection details were specified.

4.2.1 Truss

When creating the model in Abaqus, the technique of Model D decided on from Chapter 3 was used for assembling the truss. Consequently, for each truss, the instances were merged into three different parts consisting of the top chords, bottom chords, and middle section. Although the larger MAKU truss not only contained diagonal elements but also vertical ones, the middle section was maintained as one part including both diagonals and verticals. Some uncertainty arose regarding the welding of the diagonals to the upper chords, and whether the UPEs were welded to each other at their meeting point. If connected, they would be able to transfer load between one another. Due to the uncertainty, a conservative estimate was made where they are not welded together. Since the merge function in Abaqus combines the intersecting instances as described in Chapter 2.4.4, a minor distance of less than 1 mm was implemented between the diagonal UPE beams in their meeting point at the upper chords, to ensure that the diagonals remained unconnected.

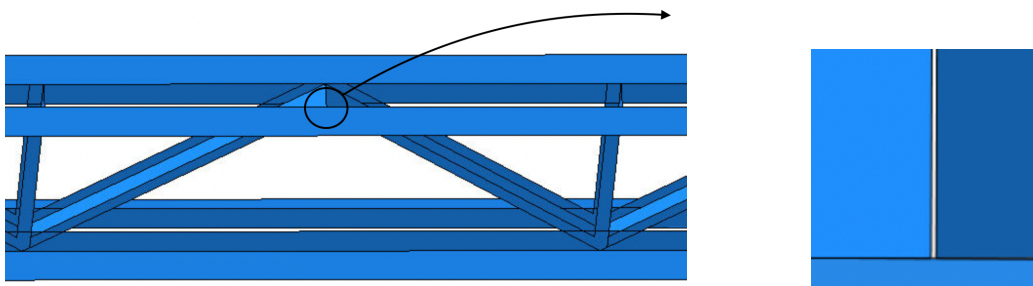


Figure 4.6: Distance between UPE beams at the upper chords.

4.2.2 Connection of Truss to Column

When creating the connection to the columns issues arose regarding the interactions and behaviour. The short HEB support was tied to the sides of the L chords in all intersecting nodes, while the bottom section was tied to the lying UPE beam. The main challenge was to simulate the interaction between the UPE beam and the underlying steel plate. When exposed to compressive force the underlying plate will directly receive the force. In tension, the bolts connecting the two parts will take the load, see Figure 4.7.

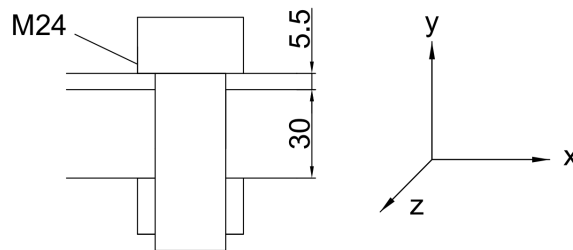


Figure 4.7: Bolt attaching the UPE beam to the plate.

To model the mechanics in Abaqus a contact property between the plate and UPE beam was used. It ensures that the UPE beam is not able to penetrate through the plate, but does not tie them together, meaning that displacements are allowed in any other direction. Complementary, a connection was used to simulate the two bolts according to Figure 4.4b. Its stiffness was set to represent the axial stiffness of the M24 bolt. The length was set equal to the thickness of the UPE web and plate combined in the y -direction as seen in Figure 4.7. It corresponds to a stiffness of 2.68 GN/m, which was only used in tension since the contact property would take the compressive forces. The x - and z -directions of the connectors were set to an arbitrary large number of 10 GN/m.

The plate was modelled with a thickness of 0.1 m to eliminate risk of local buckling occurring in the plate during simulations. It was in turn connected to the columns which were represented by line elements. A reference point in the middle of the plate was tied to a node at the top of the column. All sections of the connection between the truss and column can be seen in Figure 4.8.

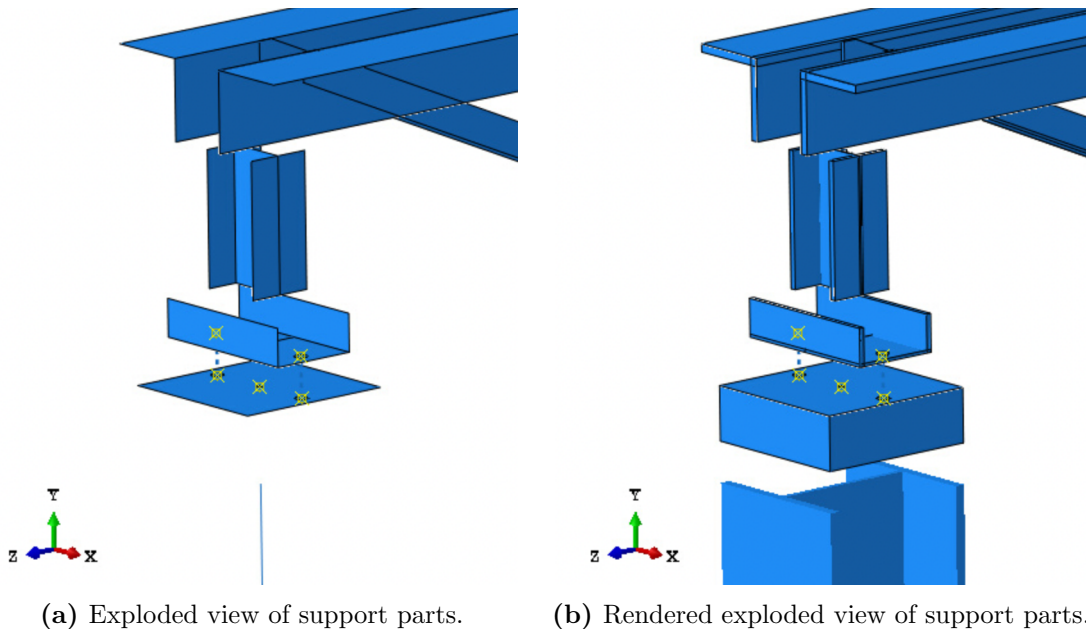


Figure 4.8: Exploded view of the parts that together connect the truss with the columns. The dashed lines represent the connectors containing the bolt stiffness, while the yellow symbols represent the reference points for connection.

Since the columns were represented by line elements, they were assigned a beam section. The section of the HEB was positioned with the stiff direction in the same direction as the truss's span as seen in Figure 4.8b.

4.2.3 CGI Roof

The CGI roof was created with the correct geometry seen in the drawings from the manufacturer Ruukki, including all minor details. As mentioned previously it had a thickness of 0.8 mm.

The roof was placed with its stiff direction according to Figure 4.1b. Since the roof

had a pitch of 280 mm between the crests it could not be made with the exact length of the truss of 26.54 meters. Since the truss was of more interest than the roof, it was therefore made slightly shorter than the truss to ensure its geometry was cut at a trough. The max width of the roof was 26.37 meters, with a total of 95 crests, without having an overhang.

According to Appendix B the roof was attached to the underlying beam at every trough. Moreover, it was only bolted to one side of the beam, in this case translating to only being attached to one of the L-flanges on which the roof rests. A modelling approach similar to the one made for the connection between the UPE beam and plate was used. Connectors were applied at the bolt locations between the upper L beam and the roof and were given arbitrary stiffness values in all three directions. Trials showed that rotation stiffness in the bolts had no large impact on the result and buckling shapes, hence these were neglected and set to zero.

A multi-point constraint was used with a function named fasteners. They work similarly to the connectors but allow for easier modelling when the connections are placed in a regular pattern. Initially, attachment points are created at the bottom surface, being the L-flange, at all spots where the bolts would be. Next, the points were assigned to attach to the nodes of the roof which were in the same vertical alignment as the points in the L-flanges. The method requires more alertness since there is less control over which nodes are attached, but with caution, it's a more time-efficient approach than manually assigning which points should be attached.

As it was noticed that the edge along the x -direction was far more prone to buckle first in comparison to the remaining structure, these were made thicker than the remaining roof. Hence, the thickness of the trough on each side of the roof was set to 5 mm. Specifically which parts were made thicker is clarified in Figure 4.9.



Figure 4.9: Thickness of roof scaled 3 times thicker than actual width, where the edge is 5 mm and remaining 0.8 mm.

4.2.4 Boundary Conditions

The columns were assumed fixed to the ground during the simulations and no displacement or rotation were allowed. This was to simulate the behaviour of foundations which are used to attach the structure to the ground.

In an actual building, the columns are connected with beams and diagonals for stabilisation purposes. To simulate this in Abaqus, boundary conditions were applied at the top of the supporting columns to replicate the connecting beams between the trusses. Displacement along the x -axis was restrained for these points since the connecting elements and bracing hinder the movement of column tops.

4.2.5 Load Definitions

The model's self-weight could be defined in Abaqus by using gravity. The gravity coefficient was set to 9.81 m/s^2 . Surfaces which represented bolt connections were ignored when assigning gravitational load due to limitations of the program.

Due to the geometry of the roof and the definition of surface forces in Abaqus, the force has to be recalculated. When adding surface traction in the program, it's not possible to define the load per measure unit of the plane but instead, it's added per measure unit of the surfaces it acts on. Since the roof has a geometry that doesn't lie flat on the plane it results in a larger force in the plane than the one assigned in the program. The force has to be recalculated with a factor to represent the load aimed to add in the plane, see Figure 4.10.

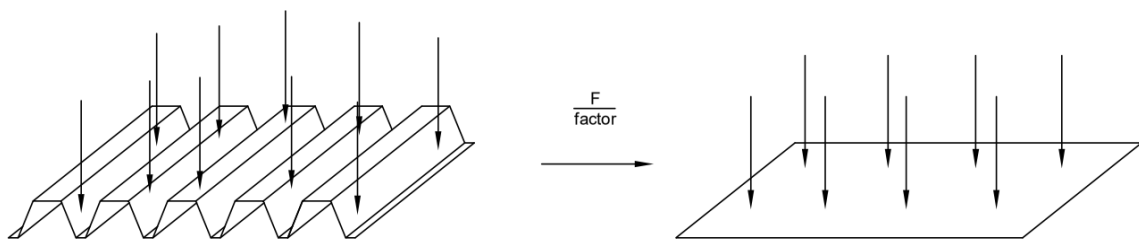


Figure 4.10: Recalculation of load with a factor to obtain a distributed load which lies on the plane.

The geometric factor added by the roof was calculated by adding a surface load on the roof of one unit load. It corresponded to a unit load of approximately 1.762 in the plane. To get the desired load per square measurement, the load would hence be divided by a factor of 1.762. For instance, to get a distributed load of 1 kN/m^2 the assigned load in the program would have to be approximately 0.5675 kN/m^2 .

4.3 Trials

4.3.1 One Truss

A version of the model containing one steel truss supported by two columns was created. The purpose of the simplified model was to get an understanding of the trusses' loading capacity and buckling behaviour without the complexity of the industrial building.

When assembling the truss structure the process of Chapter 4.2 was used while ignoring the subchapter on adding the CGI roof.

Though the truss was analysed independently, simplified stabilisation given by the columns and their connections was desired. The boundary condition in the x -direction on the top of the columns was therefore added to simulate the support of the horizontal brace between the columns perpendicular to the truss. No stabilisation provided by the roof was added as the trusses independent capacity when connected to the columns

was of interest. It serves as a reference when assessing the influence of stabilisation given by the roof.

Self-weight and live load were added. The program automatically calculates the self-weight by using the density and section assignments given by the user. Due to the lack of a roof, the live load was added on the top of the L-flanges. It was set to being 1 kN/m^2 as if the roof was lying on top of the truss. Since the influential area of the roof was larger than the area of the top L-flanges, the load was recalculated to represent the desired load. With the influential width for one truss along with the length of the roof the total load for one truss is calculated to 158.22 kN . Distributed on the flanges, it gives 19.87 kN/m^2 .

When investigating the buckling modes, nonlinear behaviour was of interest, hence an initial static and nonlinear step was defined. The step **Static General** was used as the first step in Abaqus where geometric nonlinear effects were engaged. In the step only the gravitational load was added to simulate how the building would displace and rotate when initially being assembled. The step gradually adds the load with every increment until the full load assigned has been added.

After the static step, a buckling analysis step was defined. As described in the Abaqus theory, the **Buckling** step will use the final increment of the static analysis as an initial state for all iterations being made. The imposed load, described previously and set to 19.87 kN/m^2 , was added in the buckling step.

The mesh size of the model was set to 30 mm as concluded in the mesh convergence analysis in Chapter 3.

To get an understanding of the performance of the truss, a calculation regarding the truss utilisation ratio was conducted. Chapter 6 in Eurocode 3 was utilised and the ratio was decided by calculating the reduction factor according to Equations 2.3-2.5. Firstly, M_{Rd} and M_{cr} had to be calculated.

The design moment resistance of a structural member is calculated according to Equation 4.1 where A is the cross-sectional area of the investigated member, f_y is the yield strength of the used material, and H is the moment arm. This equation is important for determining the capacity of members to carry loads safely within their elastic range. In this case, the design moment capacity is being calculated for one truss, see Figure 4.11.

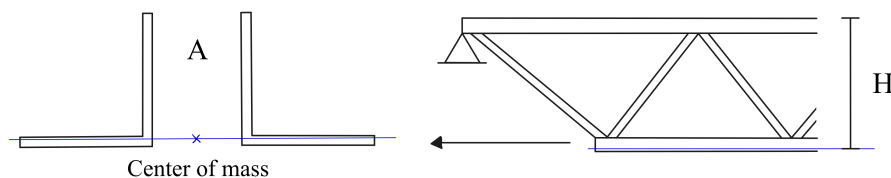


Figure 4.11: Description of parameters used for M_{Rd} .

The cross-sectional area would be either of the bottom or top chords as these are the ones to buckle in the modes of interest. Since they share the same area, it was

calculated to $A = 8.55 \cdot 10^{-3} \text{ m}^2$. The steel quality was set to 355 MPa. Likewise as for the area, the top and bottom chords were of interest when setting the moment arm H . It was set between the centre of mass for the top chords to the same point in the bottom chords which gave a height of 1.0715 m.

$$M_{Rd} = A \cdot f_y \cdot H = 3\,252 \text{ kNm} \quad (4.1)$$

The critical moment of a structural member, M_{cr} , is determined from Equation 4.2, where q_g is the load caused by the member self-weight, q_{live} is the evenly distributed live load, L is the distance between the supports, and λ is the eigenvalue obtained from buckling analysis. The length was set to the truss length of 26.54 m. The distributed loads were multiplied with the influential width of the roof by 6 m, which gave a value of approximately 6.0 kN/m due to rounding of the calculations. From the static step in the simulation, the gravitational force could be extracted. It was a total force of 62.6 kN, corresponding to 2.36 kN/m when evenly distributed.

$$M_{cr} = \frac{(q_g + \lambda \cdot q_{live}) \cdot L^2}{8} = 208 + 525\lambda \text{ kNm} \quad (4.2)$$

After the analysis was run, the first positive eigenvalue λ was extracted to obtain the critical moment. The calculated moments were then used to estimate the utilisation ratio.

4.3.2 Industrial Building with Three Trusses

A model consisting of an industrial building with three trusses was made after the testing of one steel truss was completed. This was to simulate the behaviour of how a truss functions in a whole building where there are trusses on both sides contributing to the stability of the middle one. The trusses were connected by a CGI roof with a distance of 6 meters between the trusses.

Likewise as in the previous analysis, the structure was assembled according to Chapter 4.2. Furthermore, the simulation was conducted using two steps. In the initial step, the building's self-weight was applied. Subsequently, the buckling analyses were made in the second step. Again the surface load was added in the buckling step to analyse how the building reacts to the imposed load.

In the trials, different load cases were simulated to investigate variants of buckling behaviour, see Figure 4.12. In addition to the loads previously mentioned a horizontal load was also applied to the building to account for external nonlinear impacts such as imperfection in assembly. Moreover, the occurrence of non-uniform load distribution on the roof was of interest to consider situations such as snow pockets. These two scenarios were combined in the load case trials. To create the worst-case conditions for the middle truss, two horizontal point loads of a total of 1 kN were added to the bottom middle section of the truss, displacing it to one side. Simultaneously the distributed load on the roof was only concentrated on one side of the middle truss,

creating an asymmetrical load. The side with the distributed load was the opposite side of which the truss was dragged by the horizontal load, forcing the truss to rotate further in the same direction. It was done on both sides, creating a total of three different load cases.

1. Gravity of structure included in the Static step, along with an evenly distributed load acting during the buckling step.
2. Gravity of structure included in the Static step along with a horizontal load of 1 kN placed in the middle of the mid truss dragging to the left. In the Buckling step, the distributed load was only added on the right side of the middle truss.
3. Gravity of structure included in the Static step along with a horizontal load of 1 kN placed in the middle of the mid truss dragging to the right. In the Buckling step, the distributed load was only added on the left side of the middle truss.

All scenarios can be visualised in Figure 4.12.

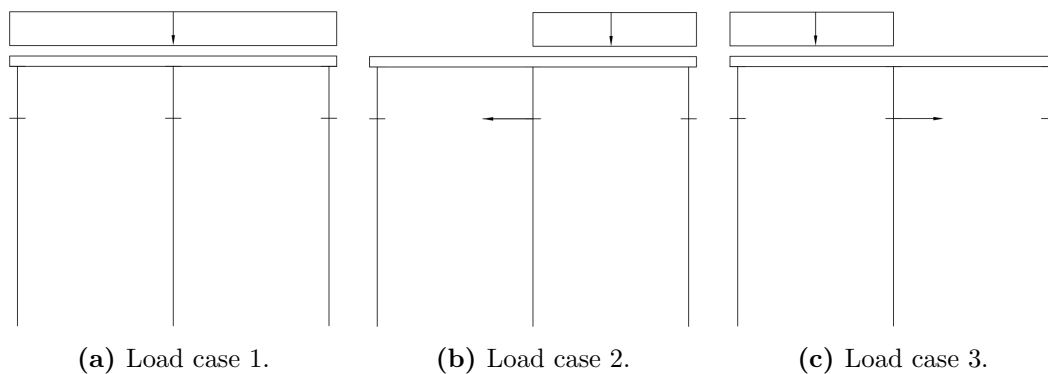


Figure 4.12: Load cases investigated when analysing the truss’s behaviour in the industrial building.

A simulation of how the building would act if the roof had been made thicker was also conducted. The thickness was set to the largest value from Ruukki which was 1.5 mm. Yet again the load cases were utilised, although the horizontal load was ignored due to Abaqus being unable to perform the simulation when it was included. Still, asymmetry was taken into consideration due to the load distribution on the roof being uneven in cases 2 and 3. Hence, the cases were equal to Figure 4.12 in terms of distributed load while neglecting the horizontal load. The result was compared to theoretical strength using Eurocode 3.

4.3.3 Parametric Study of One Truss

The results from investigating the industrial building gave little information regarding the buckling resistance of the truss as the roof seemed to buckle instead, additionally described in Chapter 4.4.2. Therefore, a parametric study was conducted to further investigate the effect of the roof on the stability of the truss.

A single truss model was constructed. Circular partitions, each with a diameter of 24 mm, were implemented to mimic the screw connections between the roof and truss. These partitions were linked to a central reference point on the surface which was in turn connected to ground via connectors. This setup allowed for the manipulation of stiffness across all six degrees of freedom, enabling a better understanding of how the roof's stiffness could affect the truss buckling.

Not all six degrees of freedom were deemed to be affected by the roof. With the axes defined according to Figure 4.16 and the z -axis in the direction of the truss, the displacement in the x -direction along with the rotation around the z -axis were identified as the two large contributors from the roof. Some other degrees of freedom were considered to be impacted by the roof, such as rotation around y -axis, although these were considered to have less of an impact on the buckling of the truss. Furthermore, they could also be dependent on the movement of the surrounding trusses in a building, such as displacement in the z -direction.

The stiffness of the rotation around the z -axis relies on the stiffness of the roof. Hence, values ranging from 0 to rigid were tested to evaluate the impact of the rigidity of the roof. The displacement in the x -direction is influenced by the thickness chosen of the roof. It could also be affected by the movement of the surrounding trusses. Therefore the axial spring stiffness in x , k_{ax} , was also varied with different values. For every value of axial stiffness in the x -direction, the varied rotational stiffness around the z -axis, k_{rz} , was tested.

To estimate the efficiency of the roof when stabilised, k_{ax} and k_{rz} were calculated from three different thicknesses of the Ruukki roof. These were 0.8 mm, 1 mm, and 1.5 mm. Their moment of inertia was extracted from the manufacturer's product catalogue. The area was calculated for a cross-section between the middle of two troughs, a width of 280 mm as shown in Figure 4.5, since it was the influence area in the x -direction of the bolts connecting the roof to the trusses. Values from the catalogue and calculations are found in Table 4.2.

Table 4.2: Cross-section area and moment of inertia for three different thicknesses of the Ruukki roof T153-40L-840.

Thickness (mm)	A_x (mm ²)	I_z (mm ⁴ /mm)
0.8	396	3 849
1	496	5 045
1.5	743	7 732

With a length of 6 metres between trusses, the axial stiffness was calculated according to

$$k_a = \frac{E \cdot A}{L} \quad (4.3)$$

The roof stiffness in the Z -direction was assumed to be equal to the moment acting at the supports, see Figure 4.13.

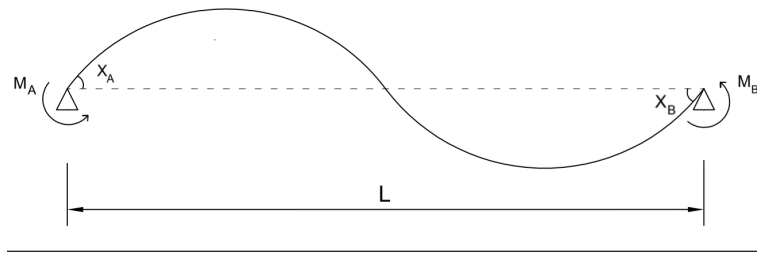


Figure 4.13: Moment at supports when calculating rotational stiffness.

The rotational stiffness of a simply supported beam can be calculated according to Equations 4.4 - 4.6

$$M_A = \frac{2 \cdot E \cdot I}{L} \cdot (2 \cdot X_A + X_B) \quad (4.4)$$

$$M_B = \frac{2 \cdot E \cdot I}{L} \cdot (2 \cdot X_B + X_A) = 0 \rightarrow X_B = -0.5X_A \quad (4.5)$$

$$\text{if } X_A = 1 \text{ rad in Eq. 4.4} \rightarrow k_r = M_A = \frac{3EI}{L} \quad (4.6)$$

When calculating the rotational stiffness of the roof its support conditions were taken into consideration. The roof can be seen as continuous and simply supported over three supports, see Figure 4.14. Since the previously calculated stiffness is over two spans, k_{rz} was calculated according to Equation 4.7

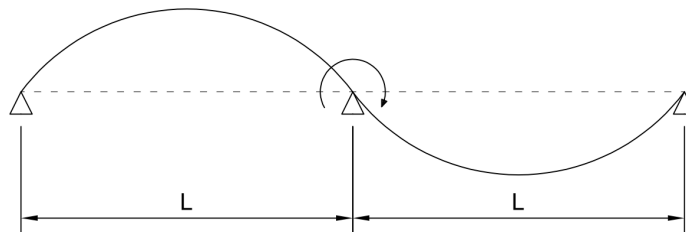


Figure 4.14: Support conditions of the roof when calculating rotational stiffness by middle truss.

$$k_{rz} = 2 \cdot \frac{3EI}{L} = \frac{6EI}{L} \quad (4.7)$$

4.3.4 Alternative Modelling Approaches

Obtaining positive eigenvalues from the parametric study which revealed truss rotation proved challenging. The results obtained from analyses according to descriptions in Section 4.3.2 and 4.3.3 differed. To delve deeper into the issue, another approach was conducted to model the effect of the roof without including the roof in the assembly. The previous model was built using springs and defining their axial and rotational stiffnesses. In the alternative approach, boundary conditions were established as a substitution for springs.

The fixed displacement and rotation boundary condition can not be given a variety of stiffnesses but only be used to set chosen degrees of freedom to fixed. Hence, the model cannot be used to investigate the influence of varying stiffnesses on the truss's stability. Instead, it was used to compare how different ways of implementing support conditions could affect the final result. Since issues arose when increasing the axial stiffness in the x -direction, only this degree of freedom was fixed in the versions. The simulations solely used the **General static** step where contact and the live load were implemented on the truss with increment steps. The live load consisted of two loads, one evenly distributed load on the top chord of the truss identical to the one used in the parametric study. The other load was a horizontal load applied in the middle of the bottom chord of the truss to force the rotation of the structure, similar to load case three Chapter 4.3.2. The increment data was analysed regarding displacement along the x -axis in relation to applied horizontal force. The reduction factor was calculated according to Equations 2.3 - 2.5.

A total of four different versions of applying the boundary conditions on the top flange were simulated. These included fixing the location of:

1. Circles created on the flange in the parametric study, where springs previously had been used.
2. Entire surface of the flange.
3. Inner edge of the flange.
4. Outer edge of the flange.

Visualisation of boundary conditions 1-4 from left to right can be seen in Figure 4.15.

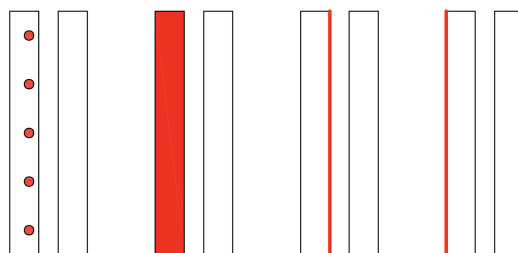


Figure 4.15: Four versions of implementing boundary conditions, seen from above truss.

4.4 Results

4.4.1 One Truss

The results from the buckling analysis show that when the load is directed with gravity, corresponding to for instance snow load, the top chord buckles. When the load is flipped and directed against gravity, a possible effect of wind load, the bottom chord will buckle. In both cases, the first mode shape start with the chord bending in one direction. With every mode found, the amount of bends increases in the chord. Figure 4.19 shows an example of a second mode. The results give insight into how the structure works and what type of result to expect from the following investigations. As the roof is attached to the top chord, its movement would be far more restricted. The bottom chord on the other hand does not obtain any further fixation when assembling the roof.

Moreover, the utilisation rate was calculated. By adding the line load of 6 kN/m, the first eigenvalue was extracted at 0.3885. It gave a critical moment of 412 kNm according to Equation 4.1. With the Eurocode equations 2.3-2.5, the reduction factor was calculated according to Equations 4.8-4.10.

$$\bar{\lambda}_{LT} = \sqrt{\frac{M_{Rd}}{M_{Cr}}} = \sqrt{\frac{3\ 252}{412}} = 2.81 \quad (4.8)$$

$$\phi_{LT} = 0.5(1 + 0.76(2.81 - 0.2) + 2.81^2) = 5.44 \quad (4.9)$$

$$\chi_{LT} = \frac{1}{5.44^2 + \sqrt{5.44^2 - 2.81^2}} = 0.099 \quad (4.10)$$

The result gives a reduction factor of approximately 9.9% when no support from the roof is available.

4.4.2 Industrial building with three trusses

After the static step had been performed, the shape due to displacement was observed and compared to the initial position since it would be the starting condition of the buckling step. Due to the modelling of the asymmetrical attachment between the top chord and the roof, the trusses deform laterally towards the side that does not contain the bolts. The stiffness in the y-direction forces the flange containing the bolts to deflect downwards together with the truss. Since no contact between the flanges and roof was modelled, the flange without bolts was not restricted to following the movement of the roof but instead followed the truss. Hence, it was in the model allowed to pass through the roof.

The results also show the effect of the horizontal load applied to the middle truss. In load case 2, the horizontal load forced the middle truss to the other side which con-

tained the bolts. In load case 3, it simply amplified the effect which already occurred in case 1. The results from all three load cases can be seen in Figure 4.16.

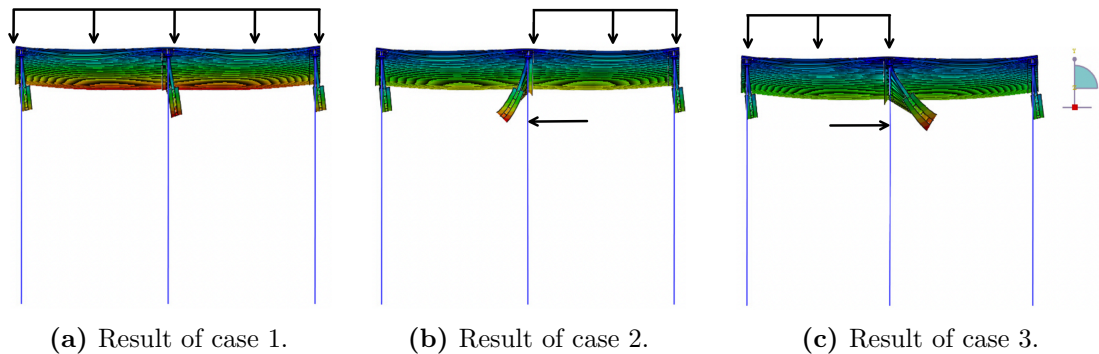


Figure 4.16: Displacements of the structure after the static nonlinear step where the difference between the load cases can be seen.

When investigating the buckling step, the general result shows that the roof appears to be the weakness of the building as it buckles first. Most mode shapes showcased a failure of the roof where the crests of the CGI roof deform by tilting to one side. The largest difference between the load cases was that in the first case when the load was applied evenly, the middle of the roof buckled. Initially, the second crest buckled and with every mode, the same buckling occurred but moved closer to the middle. In the other scenarios, the roof seemed to buckle above the truss on the side to which the load had been applied. Examples of roof buckling can be found in Figure 4.17.

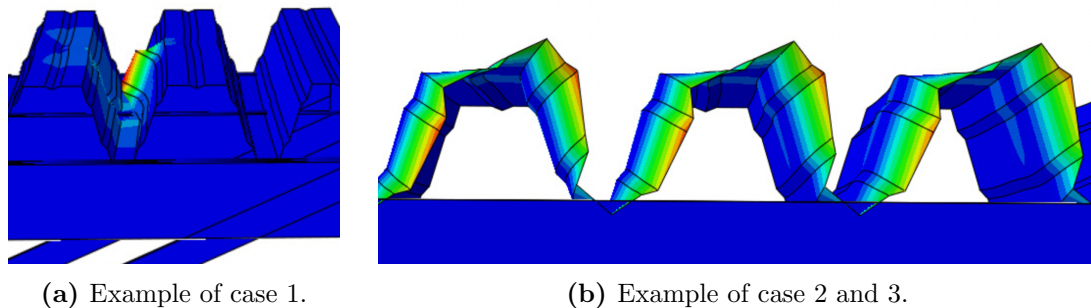


Figure 4.17: Examples of how the roof buckled

Some modes were obtained showing a buckling of the truss, however, all of these occur with a negative eigenvalue. As the value is negative it implies that the value could be valid but that the load has been switched to the other direction. The load applied to the buckling step was the distributed load pushing down on the roof, whereas with negative eigenvalues the load is pushing the roof upwards. It could for instance represent an effect from wind suction. When the truss buckled it either happened globally where the bottom chord was bent with varying amounts of curves, or locally which foremost occurred in the outermost diagonals.

As described in Chapter 4.3.2, a simulation of how the building would act if the roof had been made thicker was also conducted to potentially eliminate some of the buckling modes of the roof. The thickness was set to the largest value from Ruukki which was 1.5 mm. It successfully eliminated most of the buckling modes of the roof, although

they were almost solely replaced by negative eigenvalues where the trusses buckle. The roof buckled at the outer edge along the building's direction.

One new buckling mode of interest appeared which can be seen in Figure 4.18. It displays a buckling of all trusses with a positive eigenvalue, this was the only positive eigenvalue obtained where the truss, and not the roof, buckled.

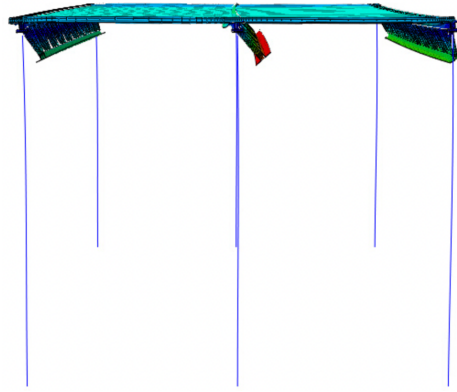


Figure 4.18: Buckling mode where the trusses buckle with a positive eigenvalue from load case 1.

The load cases showed fairly similar eigenmodes and values between the cases. Shown in Figure 4.18 was load case one. Regarding the two cases of an unevenly distributed load, the truss on the side on which the load was applied showed larger deformations while the other side barely buckled. For load case one, the live load applied at the deformation was 11.28 kN/m². For two and three it was 20.83 kN/m² and 21.32 kN/m² respectively. Although the distributed load was larger for the two latter cases, the total force was slightly smaller as the load was applied on half of the roof giving three metres as influential width.

Equation 4.1 was used to calculate M_{Rd} . The corresponding live load was calculated according to Equation 4.11 where the gravitational load of 3.58 kN/m per truss was subtracted in the calculations due to the roof load being included. It was compared to the critical load, q_{cr} , used as the live load when calculating M_{cr} , in Equation 4.2. The reduction factor was obtained from Equations 2.3-2.5, see Table 4.3.

$$q_{Rd, live} = \frac{M_{Rd} \cdot 8}{L^2} - q_g \quad (4.11)$$

Table 4.3: Load capacity and reduction factor before a truss buckles in the load cases.

Load Case	$q_{Rd, live}$ (kN/m)	$q_{cr, live}$ (kN/m)	χ_{LT} %
1	34.58	67.68	63.0
2	34.58	62.49	61.2
3	34.58	63.96	61.8

4.4.3 Parametric Study of One Truss

Since the focus of the dissertation lies on the truss, a parametric study was conducted on one truss where springs were used to model the stiffening effect of the roof. Different values of the axial stiffness in the x-direction, k_{ax} , were tested, where multiple rotational stiffnesses around z, k_{rz} , were tested for each k_{ax} -value.

As many values have been tested in the analysis, only a selection of the results is presented in here. Tables with the full result can be found in Appendix C. The corresponding eigenvalue from the mode shapes of interest was extracted and multiplied with the applied load to obtain the critical line load.

To compare the results of the parameters, four different eigenmodes were looked for and extracted. The first to be extracted was the first global eigenmode in the truss. In most cases, except when k_{ax} was set to zero or one, it was a negative eigenvalue. All chosen extracted values can be found in Table 4.4.

Table 4.4: Critical live load in kN/m from the first global eigenmode of the truss where k_{ax} of the springs is given in kN/m and k_{rz} of the springs in kNm/rad.

Rotational Stiffness Z	Stiffness X 0	Stiffness X 1	Stiffness X 10	Stiffness X Rigid
0	5.166	7.356	-17.807	-22.516
0.1	5.328	7.548	-18.067	-22.793
1	6.648	9.105	-20.112	-24.856
2.5	8.442	11.218	-22.691	-27.056
5	10.75	13.931	-25.644	-29.559
7.5	12.558	16.027	-27.673	-31.266
10	14.030	17.725	-29.187	-32.774
Rigid	16.033	20.008	-31.423	-33.965

Since the first global eigenmode became negative when k_{ax} increased, the first positive eigenvalue was also extracted. With low k_{ax} , the first mode shape resembled a global rotation of the truss around the z-axis. However, as the spring stiffness increased the first mode with a positive eigenvalue showed how the top chord was shaped like an S, see Figure 4.19.

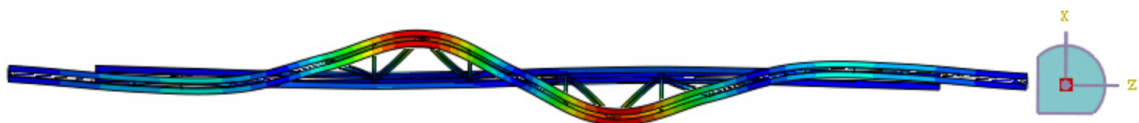


Figure 4.19: First mode shape of truss seen from above obtained with a positive eigenvalue when the axial stiffness was > 10 kN/m

Extracted values from positive eigenvalues can be seen in Table 4.5. It shows how the eigenvalue starts to increase rapidly around a k_{ax} of 10 kN/m. At the same axial stiffness but with k_{rz} of 2.5 kNm/rad, the mode shape shifts from the global rotation to an S-shape of the top chord. The last positive eigenvalue with a global mode shape was obtained at k_{ax} of 1000 kN/m. Thereafter, only local buckling occurred.

Table 4.5: Critical live load in kN/m from the first positive global eigenmode of the truss where k_{ax} is given in kN/m and k_{rz} in kNm/rad.

Rotational Stiffness Z	Stiffness X 0	Stiffness X 10	Stiffness X 1000	Stiffness X Rigid
0	5.166	20.868	102.750	Local
0.1	5.328	21.201	102.613	Local
1	6.648	23.860	102.958	Local
2.5	8.442	25.532	103.018	Local
5	10.75	27.185	103.262	Local
7.5	12.558	28.546	103.417	Local
10	14.030	29.691	103.525	Local
Rigid	16.033	31.567	103.775	Local

The first negative eigenvalue was of interest since it represents a load directed in the opposite direction, which could occur due to wind load. All mode shapes displayed a bent shape of the bottom chord, giving a global rotation of the truss.

Table 4.6: Critical live load in kN/m from the first negative global eigenmode of the truss where k_{ax} is given in kN/m and k_{rz} in kNm/rad.

Rotational Stiffness Z	Stiffness X 0	Stiffness X 10	Stiffness X 100	Stiffness X Rigid
0	-12.597	-17.807	-21.298	-22.516
0.1	-12.753	-18.067	-21.583	-22.793
1	-14.010	-20.112	-23.829	-24.856
2.5	-15.711	-22.691	-25.908	-27.056
5	-17.891	-25.644	-28.584	-29.559
7.5	-19.588	-27.673	-30.032	-31.266
10	-20.962	-29.187	-31.502	-32.774
Rigid	-22.838	-31.423	33.356	-33.965

Due to the high axial stiffness of the roof, the S-shaped mode would be unlikely to occur unless either the roof buckles or due to failure of the attaching bolts. Hence, the

positive eigenvalue where the mode shape consisted of a global rotation of the truss was also of interest, see Figure 4.20. Issues arose at k_{ax} of 100 kN/m when the mode shape no longer could be found among the eigenvalues extracted.

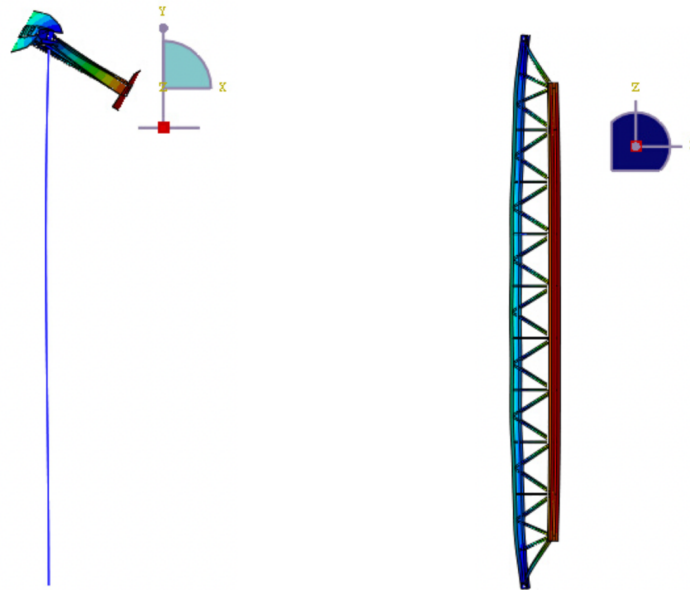


Figure 4.20: Buckling mode with lateral rotation of the truss.

Extracted values from the lateral rotational mode can be found in Table 4.7. As seen in the Table, no modes according to figure 4.20 could be obtained beyond an axial stiffness of 100 kN/m and a rotational stiffness of 5 kNm/rad.

Table 4.7: Critical live load in kN/m corresponding to eigenmode according to figure 4.20, where k_{ax} is given in kN/m and k_{rz} in kNm/rad. No found value is represented by '-'.¹

Rotational Stiffness Z	Stiffness X 0	Stiffness X 10	Stiffness X 100	Stiffness X Rigid
0	5.166	20.868	84.509	-
0.1	5.328	21.201	85.344	-
1	6.648	23.860	92.515	-
2.5	8.442	27.123	101.105	-
5	10.75	36.240	112.407	-
7.5	12.558	39.636	-	-
10	14.030	42.609	-	-
Rigid	16.033	47.202	-	-

The stiffnesses can be compared to those of the Ruukki roof to view the stabilisation of the roof. With calculations according to Equations 4.3-4.6, the stiffnesses obtained from the manufacturer can be seen in Table 4.8.

Table 4.8: Axial and bending stiffness of support springs representing different sheet thicknesses.

Thickness (mm)	Stiffness k_{ax} (kN/m)	Stiffness k_{rz} (kNm/rad)
0.8	13 876	226
1	17 345	297
1.5	26 017	455

Figures 4.21 and 4.22 present a comparison between the first positive buckling loads obtained from simulations. Figure 4.23 and 4.24 present a comparison between the first negative buckling load obtained from simulations. Please note that the negative values have been converted to positive ones to facilitate the readability of the graphs.

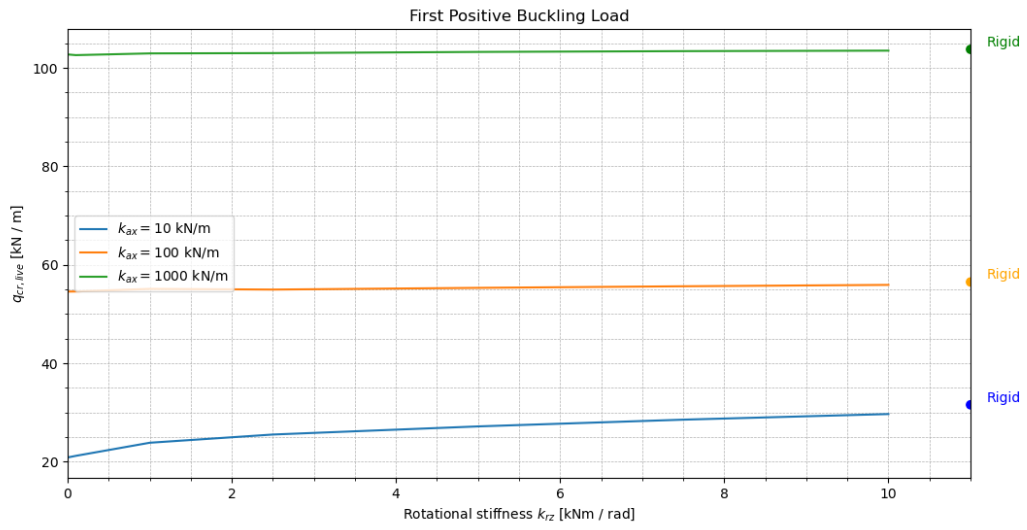


Figure 4.21: Comparison of first positive buckling load with axial stiffness, k_{ax} , of 10, 100 and 1000 kN/m.

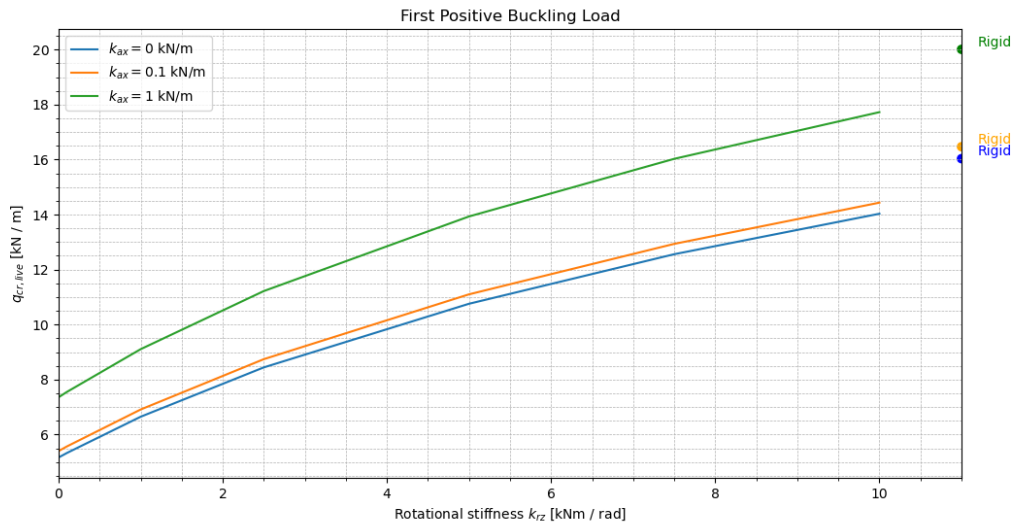


Figure 4.22: Comparison of first positive buckling load with axial stiffness, k_{ax} , of 0, 0.1 and 1 kN/m.

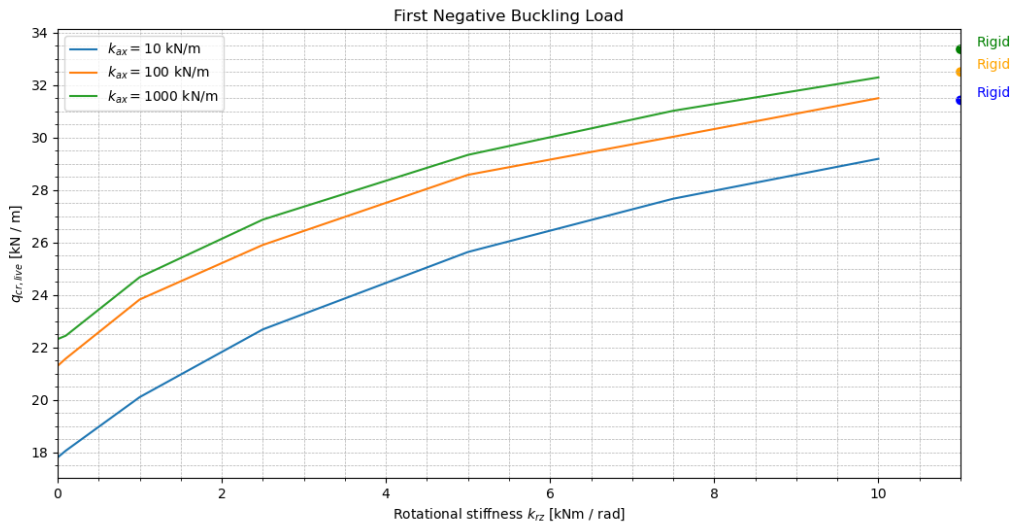


Figure 4.23: Comparison of first negative buckling load with axial stiffness, k_{ax} , of 10, 100 and 1000 kN/m.

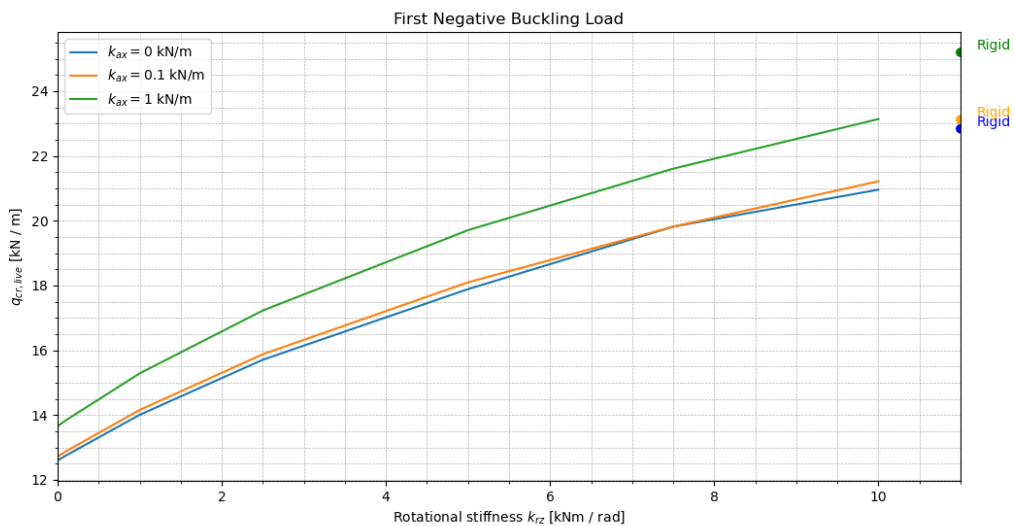


Figure 4.24: Comparison of first negative buckling load with axial stiffness, k_{ax} , of 0, 0.1 and 1 kN/m.

The obtained results show that an increased axial stiffness and rotational stiffness generally result in more stability of the truss and higher buckling loads. The rate at which the buckling load increases with rotational stiffness varies depending on the specific stiffness values and the magnitude of the increase.

4.4.4 Alternative Modelling Approaches

The simulation consisted of solely using the **General static** step. Unlike the Buckling step, it does not give an eigenvalue which can be converted to a critical load. Instead, it implements part of the applied load at every increment, eventually reaching the defined load at the end of the step.

To approximate the critical load, the displacement was extracted in the x-direction at a chosen node in the middle of the lower chord of the truss. The displacement was at every increment compared to the proportion of load being applied. The relation between the parameters can be seen in Figure 4.25 for all four approaches of applying boundary conditions.

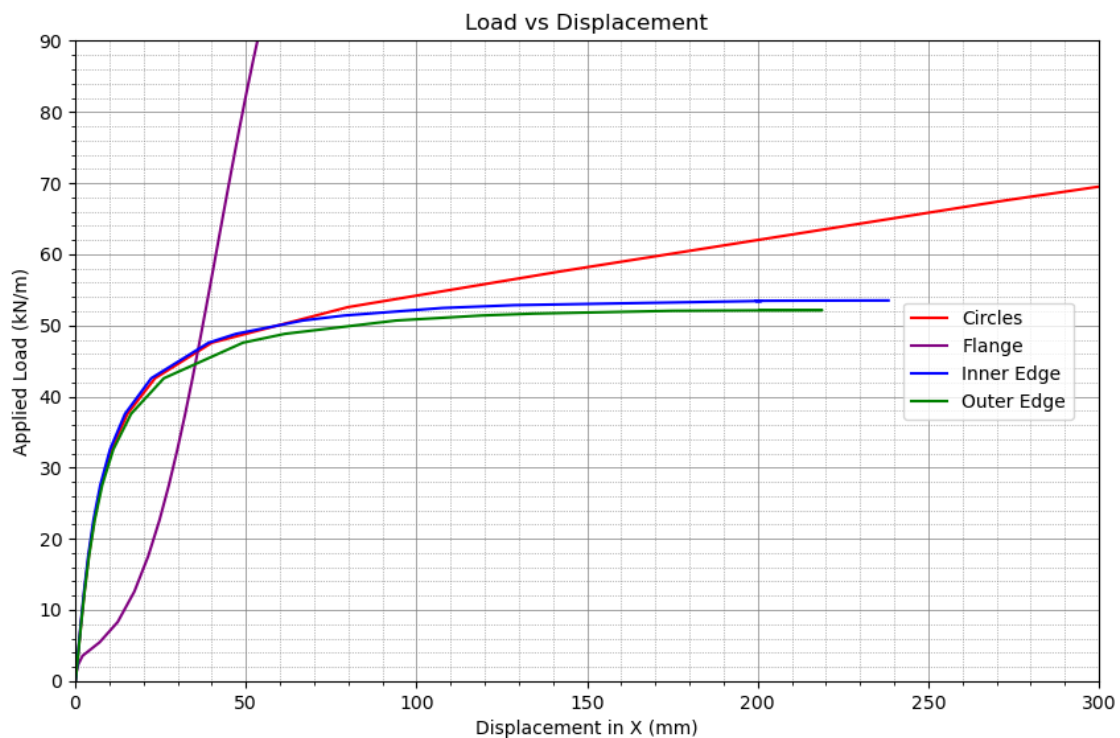


Figure 4.25: Displacement of node at location of one horizontal load as a function of distributed at horizontal load applied.

From the graph, the critical loads are approximated for each support condition. It was assumed at an arbitrary displacement of 50 mm due to the majority of curves approaching a horizontal appearance along with it corresponding to approximately 5% of the height of the truss. As seen in Figure 4.25, the approach where the full flange was fixed seems to flatten only to quickly increase vertically again. This is interpreted such that the displacement initially increases, but at a later stage, the forced rotation of the truss results in a stiffening effect. Thus it is questionable if this case is to be categorised as a critical load in the sense of (theoretically) unlimited deformation.

All alternative modelling approaches are compared between their critical load and reduction factor in Table 4.9.

Table 4.9: Obtained critical live load and reduction factor from alternative modelling approaches.

Boundary Conditions	Critical Load (kN/m)	Reduction Factor (%)
1: Circles	49	55.7
2: Whole Flange	82	67.1
3: Inner Edge	49	55.7
4: Outer Edge	47	54.7

5 Discussion

5.1 Single Truss

The analysis of the simply supported truss revealed that the structure rotates along the truss's axis, being the global z-axis. As the truss has a long span with no support between the two columns, the structure was slender and prone to buckling at low loads. It was confirmed by the low eigenvalue at which the first buckling mode appeared.

A truss of the chosen type with no support from a roof could only manage a load of approximately 2.33 kN/m before buckling. The corresponding critical moment of 205 kNm resulted in a utilisation rate of only 5.3%. It proves that the mechanical structure of the truss relies on a complementary structure to stabilise in the normal direction of the truss, being the x-direction, and for rotation along the direction of the truss, corresponding to around the z-axis.

The simulation of a single truss structure was primarily conducted to anticipate which mode shapes to expect when the roof was added. Generally, the positive eigenmodes occurred when the top chord buckled, while the negative eigenmodes were found when the bottom chord buckled. It gave insight into how the roof will stabilise the truss since it will support the top, particularly in the x-direction and rotation around the z-axis. For wind loads on the other hand the structure would be less supported if no bracing of the bottom chord was used.

5.2 Industrial Building

Difficulties arose regarding the connections between the top of the L-flanges and the roof. Initially, the method included a similar approach as the connection between the UPE beams and thick plate by the supports by using contact property in pressure and connector in tension. However, issues arose when utilising the technique as Abaqus assumed all surfaces being in contact at the start of the buckling iterations to be tied to each other. The tie could affect the result profoundly as contact in the simulations was often made on the flange which had no bolts, which made the method deemed inappropriate with unrealistic boundary conditions in the buckling step.

The solution was to remove the contact assignment and assign a larger stiffness in the y-direction in both tension and compression. It could cause a reverse effect compared to the contact as the truss now only would be restricted in displacement and rotation by the bolt connectors. An effect seen in the simulation was the roof seemingly pushing down the truss by the bolts on one flange. It triggered a rotation since the other flange had no direct interaction with the roof, giving an asymmetric load on the truss. If an interaction had been assigned it could have influenced the rotation largely both

in terms of magnitude and direction. Although the interaction was still regarded as lacking some aspects, the scenario was more conservative than the one including contact.

There was a difficulty with finding the positive eigenvalues when performing the buckling analysis. Due to the connectors used in the Abaqus model, the Subspace method had to be used for the buckling iterations. A major downside of the method is that the eigenvalues of interest cannot be restricted to an interval but at most restricted to a maximum value of interest. It deeply contributed to the issue of extracting positive eigenvalues from the simulations. The vast majority of all eigenvalues presented in the results from the simulations were negative. Moreover, many of these were local buckling. If a minimum eigenvalue could have been specified, all the negative ones could have been neglected by simply setting the minimum value to zero.

To try and provoke the middle truss to buckle, two other load cases in addition to the uniform load were tested. A combination of concentrated load horizontally acting on the truss along with an unevenly placed live load on the roof. The cases were simulating the event of imperfections of the middle truss causing it to move to one side, along with a snow pocket on the roof. Despite the different load cases, no positive eigenvalue could be found where the trusses buckled. The largest difference could instead be found in where the roof buckled. When the load was uniformly applied the buckling occurred in the middle of the roof, while in the non-uniform cases, it was found on the loaded side.

Another attempt to find the buckling load of the truss was made where the roof was made thicker to try and eliminate some of the earlier buckling modes of the roof. The thickest roof from MAKU of 1.5 mm was used. It successfully eliminated some of the eigenvalues from the roof, and a buckling mode of the truss buckling could be found for all three cases. The mode showed how all three trusses buckled, although different trusses were more affected depending on the load case. Translated to a line load for one truss, the lowest load could be applied in case two where the mode occurred at 62.49 kN/m. When a uniform load without horizontal influence was used, it occurred at 67.68 kN/m for the middle truss which was the least of the three. Hence, the difference between load cases was deemed to be relatively minor.

The reduction factor of all three cases was approximately just over 60%. Hence, a large fraction of the truss' theoretical capacity is lost due to the construction. In the physical constructions used in Sweden, the roof thickness used would most likely be thinner than 1.5 mm. As seen in Table 4.2, the axial and rotational stiffness would decrease significantly when the roof's thickness is reduced. Assuming that there is no failure of the roof, the truss would most likely buckle at a lower load and would give an even lower utilisation rate of the capacity.

5.3 Parametric Study of One Truss

The findings from the parametric study indicate that the rotational stiffness significantly influences the buckling live load of the truss, particularly when the axial stiffness,

k_{ax} , is lower. As the axial stiffness surpasses 10 kN/m, the impact of the rotational stiffness decreases in the simulation results. However, this observation did not hold for the initial negative eigenvalues of the analysis. The negative live load, representing wind force acting on the underside of the roof, consistently experiences the influence of rotational stiffness, k_{rz} . The buckling load resistance calculated from negative eigenvalues increases by an average of 10 kN/m between undefined and rigid rotational stiffness along the z-axis. This demonstrates the influence of the axial stiffness on the buckling behaviour of the truss. Upon exceeding a threshold of 10 kN/m, the significance of rotational stiffness diminishes in affecting the results, while the resistance to buckling load experiences a substantial increase.

The previous model with the industrial building corresponds to an axial stiffness of 7 285 kN/m and rotational stiffness of 3.87 kNm/rad. In the case where no horizontal load was applied, it gave a critical load of 67.68 kN/m. To compare with the parametric study, values between 1000-rigid in axial stiffness and 10-rigid in rotational stiffness would be of interest. However, Table C.8, corresponding to the twisting mode shape of interest, lacks values in the interval. The last critical load to be found for the mode shape was 112.4 kN/m at an axial stiffness of 100 kN/m. Despite the stiffness being approximately 100 times smaller than the roof stiffness, the critical load obtained was significantly larger than that obtained using the industrial building. The difference shows that the modelling approach has a crucial impact on the result given from an analysis, and should be investigated further.

Due to there only being a minor difference between the largest number and rigid in either k_{ax} or k_{rz} , no further values were tested despite the roof acquiring values in between. The calculated stiffnesses of the roof are theoretically derived and assume the full capacity of the roof being utilised until global buckling occurs. However, the attachment of the bolts would presumably lead to local buckling in the surrounding area occurring before global capacity is reached. Thus, the k_{ax} and k_{rz} can be assumed as somewhere lower than those calculated in Table 4.8 and the values in the table maximum values of the potential stiffness..

The parametric study was conducted using one truss with a simulated connection to the roof via springs. The stiffness along the building's direction (x-axis) and the rotation along the truss (z-axis) were varied while the vertical load in the upper chord remained the same. This model was created to study the roof's impact on one truss since the full building buckling behaviour was very time-consuming. One end of the springs was connected to small partitioned surfaces on the upper chord of the truss with a radius representing the screws between the truss and the CGI roof. The other end was connected to the ground and the stiffness of each spring was then adjusted according to the study. This gives relatively accurate simulations of the roof's impact on the truss stability but lacks some important factors.

The surface contact between the roof and the upper chords was neglected in this model which could have significantly affected the structural behaviour and stability of the system. Ignoring this interaction may lead to inaccuracies in the simulation results, particularly in assessing the distribution of forces, deflection, and overall structural performance. While the simulated connection via springs provides a simplified interaction between the truss and the roof, they may not capture the complex behaviour

of the actual connection. Additionally, by focusing solely on the impact of the roof on one truss, the parametric study overlooks other factors that could influence the overall stability of the building. For example, interactions between adjacent trusses, lateral bracing systems, foundation conditions and external loading conditions all play a significant role in determining the building's buckling behaviour.

The mesh size had a significant impact on the accuracy and reliability of the obtained results of the parametric study. Due to the small partitioned areas for the roof bolts on the truss, it was necessary to decrease the mesh size to run the simulations in the program. However, the smaller mesh increased the computational costs which led to longer simulations. Because of this, the mesh size was solely decreased for the upper chord of the truss where the roof bolts were simulated to make the simulations more efficient. As previously mentioned, the density of mesh size directly influences the ability of the simulations to capture local buckling mode shapes. This made it harder to find the global buckling mode shapes from the simulations which was the focus of the work.

Due to the local buckling modes, it was likewise as for the industrial building difficult to obtain the eigenvalues of interest. For lower values of the axial stiffness of the supporting springs, all four mode shapes of interest could easily be extracted. However, when the axial stiffness was at 1 MN/m, the global rotation of the trust according to Figure 4.20 could not be found among the 50 eigenvalues extracted. Due to the long simulation time in the Buckling step and the large amount of simulations, limitations had to be set to an adequate amount of eigenvalues for each study.

Although no positive eigenvalue with global buckling of the truss was acquired with higher axial stiffness, the mode seen in Figure 5.1 with columns buckled was found in all simulations. Since no axial stiffness of the supporting springs was applied in the z-direction, the mode was always obtained at the same load of 92 kN/m. The mode shape was neglected, despite sometimes being the only positive global mode, due to the truss being of interest. Moreover, the stabilisation in the z-direction remained unknown, and with bracing in the gables of the building the buckling mode would be inadmissible.

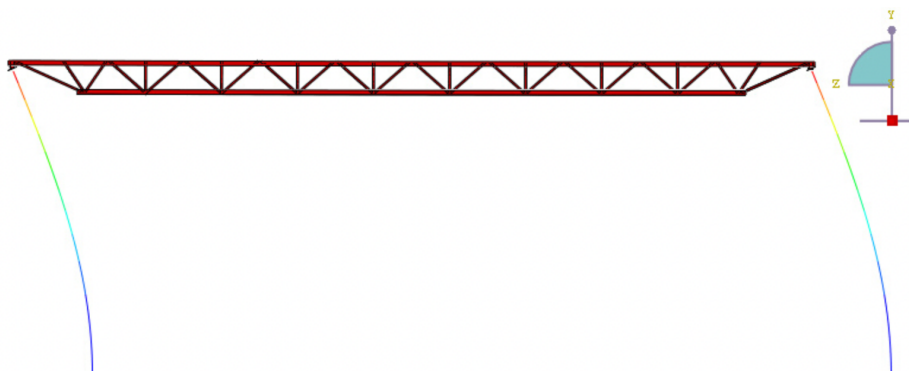


Figure 5.1: Positive buckling mode with higher axial x-stiffness.

As the parametric study was performed without a roof, the gravitational force simulated by Abaqus only included the self-weight of the truss and columns with their connecting parts. Hence, the self-weight of the roof has to be extracted from the live

load when estimating how much, for instance, snow load the construction can endure. With a roof of 1.5 mm, it would be approximately 1.22 kN/m for one truss. Other dead loads, such as installations, could also have to be taken into account.

The negative eigenvalue showed the least difference when increasing the axial stiffness of the supporting springs, although the rotational stiffness had a similar impact as for the positive eigenvalues.

5.4 Alternative Modelling Approaches

The investigation of alternative modelling approaches aimed to deepen comprehension of the spring model. Notably, each of the alternative modelling simulations demonstrated a reduced buckling load compared to the spring model, underlining the substantial influence the modelling approach has on resultant outcomes. This phenomenon may occur from different factors, such as the marginal offset of partitions within the upper chord from the centre line, potentially impeding the desired rotational eigenmodes. The reason behind the differing results may be related to the program Abaqus having difficulties finding the eigenmodes for the desired outcome.

When comparing the three different methods, the model using the industrial building and the alternative approach with boundary conditions and general step are most similar in result. Although they differ by around 10 kN/m, they are remotely closer to each other than to the parametric study.

A significant difference can be found between the different modelling approaches which proves its importance. Further investigations would have to be made to conclude which would be the result closest to reality.

Due to both step type and modelling of the roof being changed in the alternative method, it remains unclear if either one or a combination of both resulted in a different critical load to the parametric study. If the **General static** step had been used throughout the parametric study, more critical loads could have been extracted. Moreover, it could affect the influence of rotational stiffness.

5.5 Usage of Line Elements

The columns connecting the truss to the ground were modelled using line elements which brings forth certain benefits and drawbacks from the simulations. Using line elements enhances computational efficiency and simplifies the modelling process. It facilitates connectivity between the trusses and the ground.

Conversely, line elements have local limitations. They struggle to accurately represent complex behaviours like bending and buckling effects, potentially leading to inaccuracies in the simulation results. Boundary effects at connections may also affect the accuracy of the analysis.

5.6 Contribution to Previous Research

The result of the simulations with the industrial building contradicts the conclusion of the previous research of Tosovic [1]. Despite the contradiction, the results seem to differ rather in interpretation than values. When observing the result of the buckling analysis from the previous report, it can be seen that the extracting values from when the bottom chord of the truss buckles are negative. The positive eigenvalues on the other hand occur when the roof buckles, although these were deemed as local.

This work neglected negative eigenvalues when performing analyses with the industrial building. Likewise as Tosovic [1], negative eigenvalues were obtained for the cases when the bottom chord buckled. The results were primarily focused on gravitational loads such as snow loads, as these were regarded as possible causes of the collapses of similar buildings in northern Sweden. Hence, the dissertation doesn't oppose the previous result but clarifies how the capacity of the load-bearing components differs with the direction of the load.

6 Conclusion

6.1 Buckling Resistance of the Truss

The initial investigation of only the truss and its support components with the columns proves the structure's slenderness when no external stability is given. It is prone to lateral buckling under relatively low-loading conditions, shown with a low reduction factor calculated according to Eurocode 3. Further insight was given into the truss's buckling behaviour as it was seen that the top chord was more prone to large deformations in the lateral buckling as the load was directed in the direction of gravity. When the load is flipped, which could occur during wind suction, the bottom chord deforms more.

As indicated in the initial analysis, the truss was stabilised profoundly when applying the roof on the structure as the top chord became limited in movement due to the attaching bolts. The utilisation rate increased six times compared to the case without the roof. Three different load cases were investigated where uniform load and symmetry in the assembly were compared to two cases of unevenly distributed load and a horizontal force acting on the middle truss. A minor difference was found between the cases as the critical live load for all of them gave a utilisation rate of above 60%. The mode shape differed slightly as the truss experiencing the major lateral buckling varied with the load cases.

The parametric study conducted showed how the axial stiffness perpendicularly to the truss provided the largest impact on the overall buckling stability of the truss. While the rotational stiffness around the truss also provided stability, it did not give as drastic of a difference between the results. Due to the lack of results from the buckling analysis, the influence of roof choice could not be determined from the study.

When using the alternative modelling approaches the lowest utilisation rate was obtained under 50%, disregarding support case two, where the whole upper flange area was assigned boundary conditions. No conclusion can be drawn on the most realistic critical load of the truss as it differs between all methods. A conservative conclusion would be to assume the load-bearing capacity from the alternative modelling approach.

6.2 Load Capacity of Industrial Building

Although previous research states that the truss was the weakest load-bearing component and the first to buckle, the simulation of the industrial building made in this dissertation shows that the roof experiences buckling before the truss. It contributed to issues in extracting eigenmodes in which the truss buckled instead of the truss, where a thicker roof than the initial one had to be used to obtain the results.

This dissertation focused only on the positive eigenmodes when analysing the simulations using the industrial building, whereas the previous research included negative ones. Therefore, when forces act in the direction of gravity, including for instance self-weight and snow load, the roof is deemed to be more prone to buckle. During the event of opposite directional load in the case of for instance wind suction, the truss would buckle first due to instability of the bottom chord.

6.3 Modelling Approach

The dissertation proves that modelling approaches hold great significance in simulating structural problems, particularly when using advanced finite element analysis software such as Abaqus. This underlines the necessity for careful selection and validation of modelling approaches to ensure that the simulations closely replicate real-world behaviour, thereby providing more dependable insights for engineering applications.

6.4 Continued Research

As the result differed between the models with the industrial building, using springs, and boundary conditions with a different step, a study of interest would be to compare different modelling techniques in greater depth. However, it is proposed that further work should include full nonlinear analyses as a reference, as linear buckling procedures are not relevant to use in combination with contact modelling.

This dissertation only examined the influence between the choice of elements slightly in Chapter 3, when the model using some line elements was compared to those using only shell. A further study of the impact between element choices, also including 3D elements, would be of interest.

Another common structure of industrial buildings in Sweden includes using secondary girders perpendicular to the truss and placing these evenly distributed on the truss. The roof is placed on top of the girders with the direction switched, meaning the stiff direction follows the line of the truss. It introduces eccentricity in the structure, possibly creating further instability. A similar analysis could be made of the structure type and comparing it to the structure analysed.

A further investigation could be made using the results and comparing the acquired critical live loads to those acting on some cases of collapsed buildings in northern Sweden. This could provide insights into the reasons for the collapses occurring, and whether these were overloading the structure capacity, or whether it was most likely due to faultiness in the construction phase.

According to the simulations of the industrial building, the reduction factor showed a conservative utilisation rate of approximately 55% for the current structure. A study on optimising the truss structure could be appropriate for continued research to potentially find a solution with a higher utilisation rate.

Bibliography

- [1] Nikola Tosovic. *Stability Analysis and Modelling of a Structure with Corrugated Roof*. Tech. rep. Division of Structural Mechanics, Faculty of Engineering LTH, Lund University, 2020.
- [2] Victor Omotoriogun. *Design of Steel Trusses to EUROCODE 3*. Structure Center, 2021.
- [3] Sky Civ. *Why Are Trusses So Efficient Over Long Spans*. Accessed on 8 May 2024. 2019. URL: <https://skyciv.com/technical/why-are-trusses-so-efficient-over-long-spans/>.
- [4] Katrin Hanses. *Basics Steel Construction*. Birkhäuser, 2015.
- [5] American Institute of Steel Construction. “Why Steel”. In: (2024).
- [6] Niels Ottosen and Hans Petersson. *Introduction to the Finite Element Method*. Pearson Prentice Hall, 1992.
- [7] M. Ristinmaa and M. Wallin. *Introduction to Non-linear Finite Element Method*. Division of Solid Mechanics at Lund University, 2022.
- [8] M.Reza Eslami. *Buckling and Postbuckling of Beams, Plates, and Shells*. Springer International Publishing AG, 2018. DOI: 10.1007/978-3-319-62368-9.
- [9] Dassault Systèmes. *Abaqus 2016 Documentation*. Accessed on 27 February 2024. SIMULIA. 2016. URL: <http://130.149.89.49:2080/v2016/index.html>.
- [10] C M Wai, Ahmad Rivai and Omar Bapokutty. “Modelling Optimization involving Different Types of Elements in Finite Element Analysis”. In: *IOP Conf. Ser.: Mater. Sci. Eng* (2013). DOI: 10.1088/1757-899X/50/1/012036.
- [11] Zardadkhan Irfan. “Simulation: Shell Elements vs. Solid Elements”. In: *Javelin* (2012).
- [12] Maria Augusta Neto, Ana Amaro, Luis Roseiro, José Cirne and Rogério Leal. *Engineering Computation of Structures: The Finite Element Method*. Springer International Publishing Switzerland, 2015. URL: [https://link.springer.com/chapter/10.1007/978-3-319-17710-6_7#:~:text=A%20three%2Ddimensional%20\(3D\),extension%20of%202D%20solids%20elements,.](https://link.springer.com/chapter/10.1007/978-3-319-17710-6_7#:~:text=A%20three%2Ddimensional%20(3D),extension%20of%202D%20solids%20elements,.)
- [13] Dassault Systèmes. *Abaqus*. Accessed on 27 February 2024. n.d. URL: <https://www.3ds.com/products/simulia/abaqus>.

Appendix A

Detail Drawings from MAKU

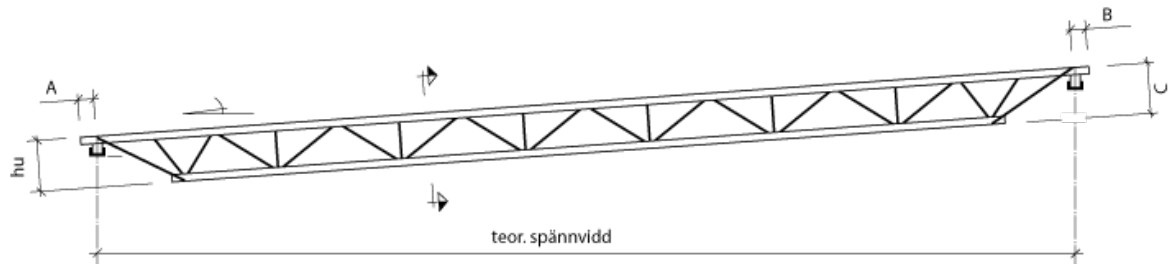


Figure A.1: General structure of truss.

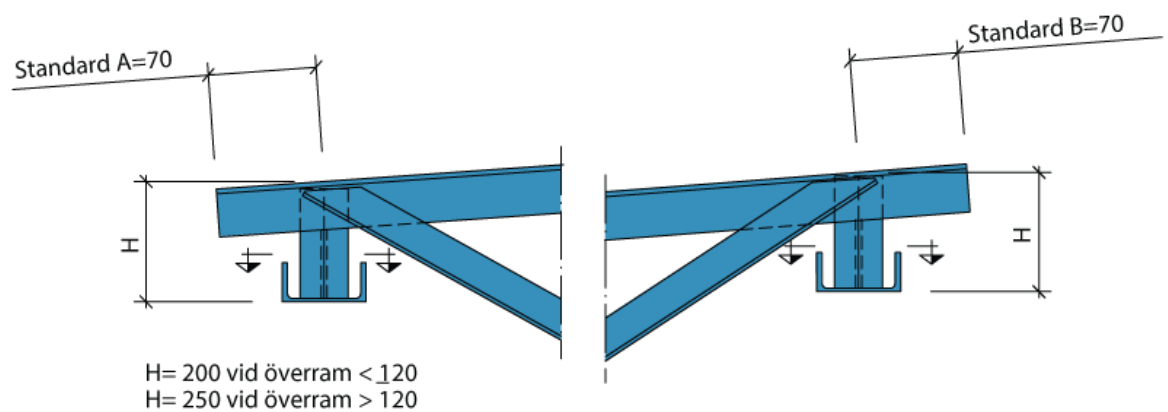
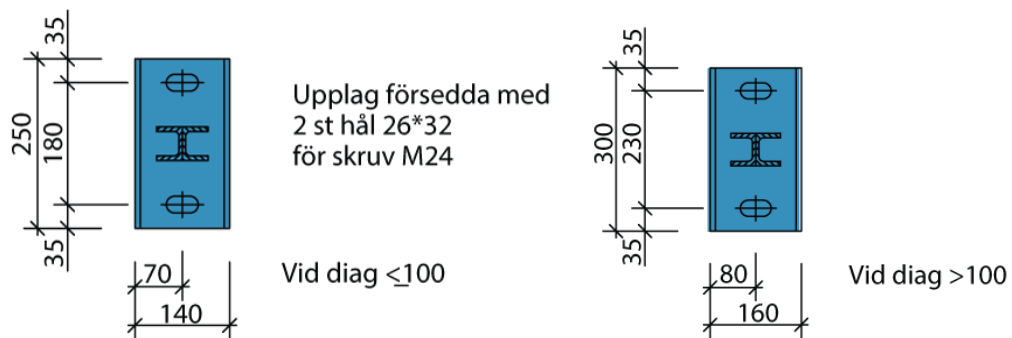


Figure A.2: Edges of truss.



(a) Size with smaller section of diagonals.

(b) Size used in dissertation.

Figure A.3: Section by UPE support that connects truss to column.

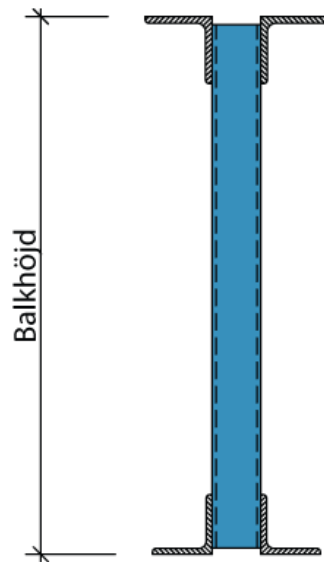


Figure A.4: Section of truss.

Appendix B

Detail Drawings from Ruukki

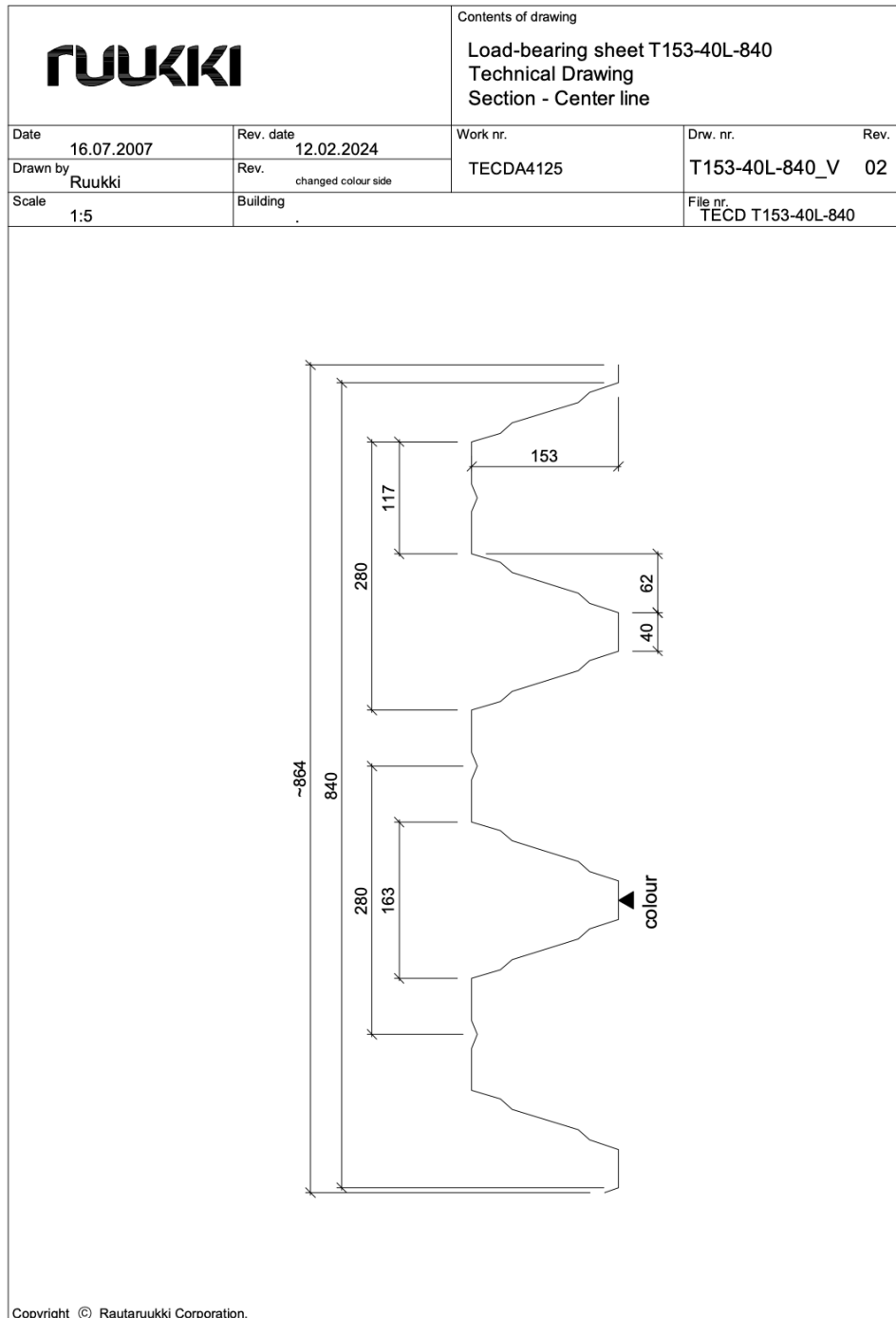


Figure B.1: Section with measurements of the pattern.

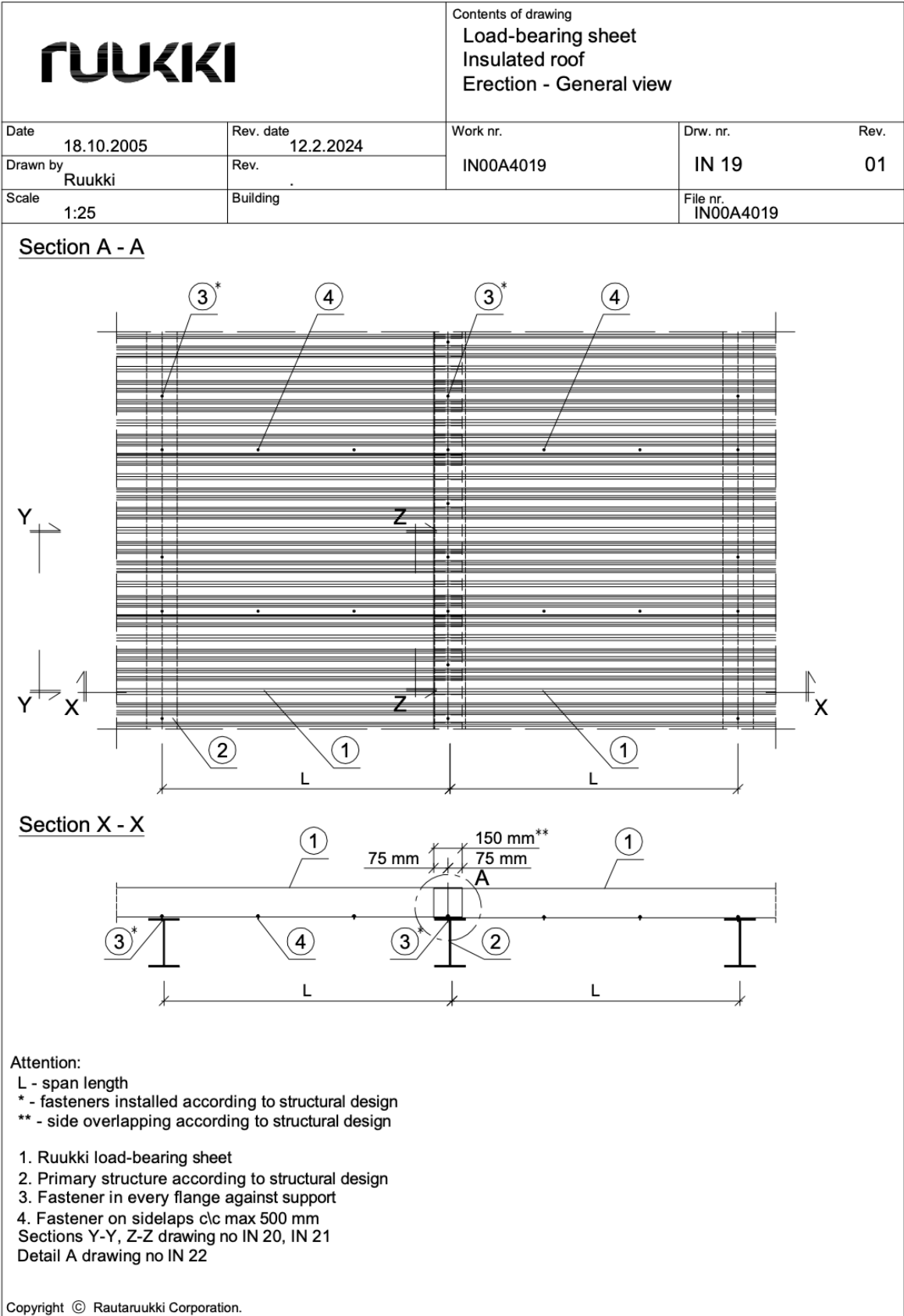


Figure B.2: Attachment of roof to underlying construction, also showcasing overlapping roof.

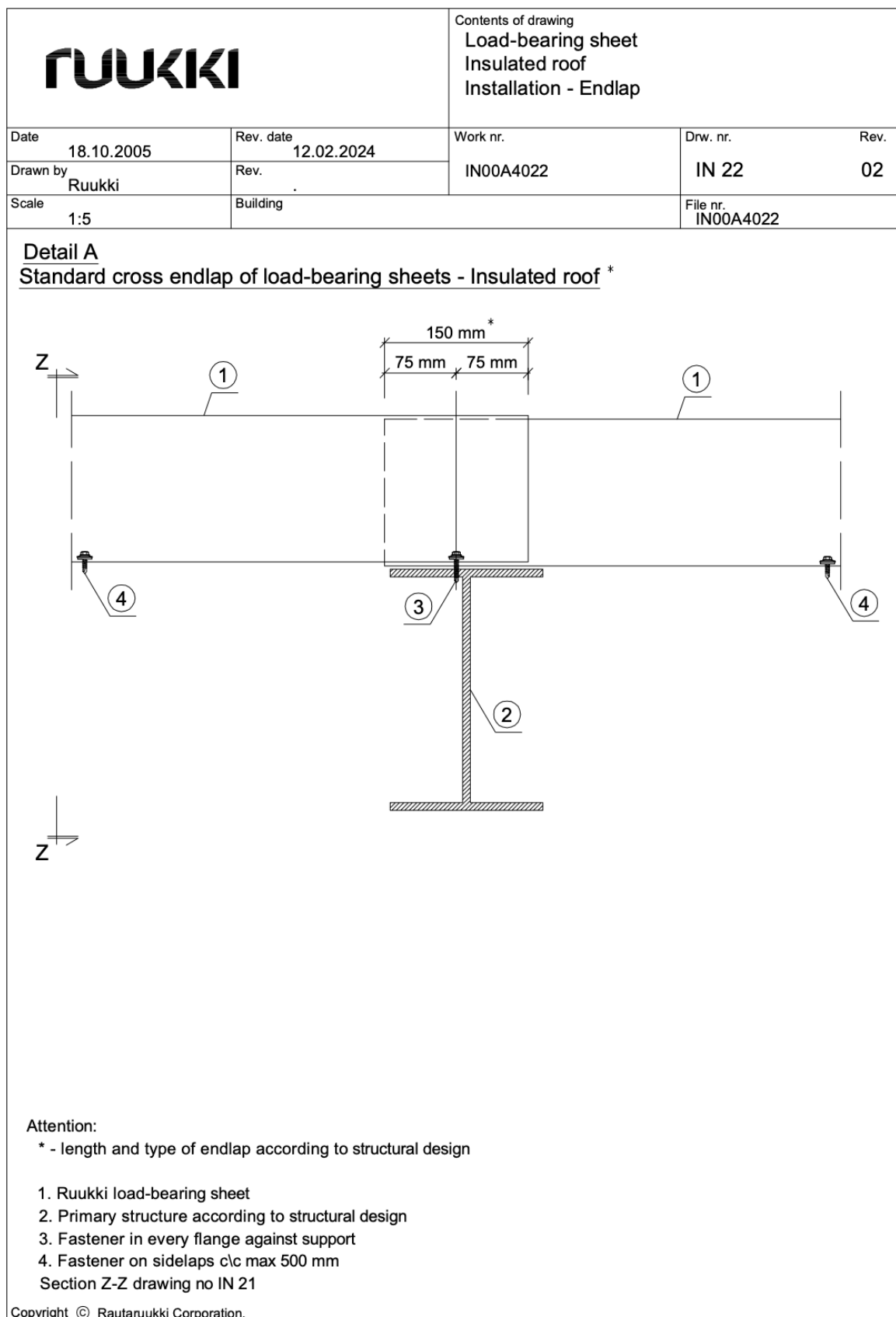


Figure B.3: Close up on placement of bolt to the underlying construction.

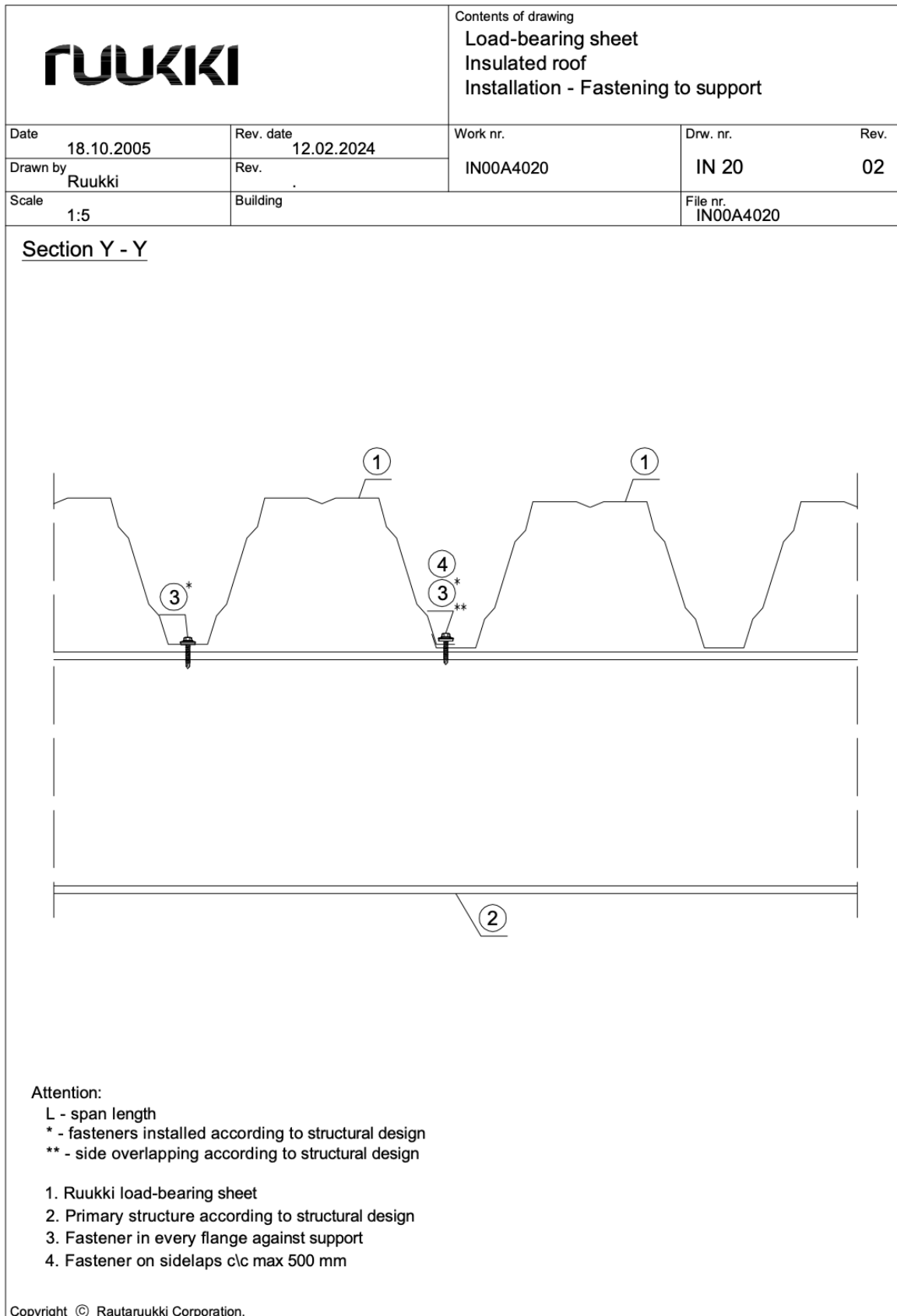


Figure B.4: Close up on regularity of bolt placement on the roof to underlying construction.

Appendix C

All Result from Parametric Study

Table C.1: Critical live load in kN/m from the first global eigenmode of the truss where k_{ax} of the springs is given in kN/m and k_{rz} of the springs in kNm/rad.

Rotational Stiffness Z	Stiffness X 0	Stiffness X 0.1	Stiffness X 1	Stiffness X 10
0	5.166	5.400	7.356	-17.807
0.1	5.328	5.566	7.548	-18.067
1	6.648	6.911	9.105	-20.112
2.5	8.442	8.741	11.218	-22.691
5	10.756	11.099	13.931	-25.644
7.5	12.558	12.934	16.027	-27.673
10	14.030	14.433	17.725	-29.187
Rigid	16.033	16.468	20.008	-31.423

Table C.2: Critical live load in kN/m from the first global eigenmode of the truss where k_{ax} of the springs is given in kN/m and k_{rz} of the springs in kNm/rad.

Rotational Stiffness Z	Stiffness X 100	Stiffness X 1 000	Stiffness X Rigid
0	-21.298	-22.319	-22.516
0.1	-21.583	-22.447	-22.793
1	-23.829	-24.679	-24.856
2.5	-25.908	-26.873	-27.056
5	-28.584	-29.341	-29.559
7.5	-30.032	-31.018	-31.266
10	-31.502	-32.291	-32.774
Rigid	-32.501	-33.356	-33.965

Table C.3: Critical live load in kN/m from the first positive global eigenmode of the truss where k_{ax} is given in kN/m and k_{rz} in kNm/rad.

Rotational Stiffness Z	Stiffness X 0	Stiffness X 0.1	Stiffness X 1	Stiffness X 10
0	5.166	5.400	7.356	20.868
0.1	5.328	5.566	7.548	21.201
1	6.648	6.911	9.105	23.860
2.5	8.442	8.741	11.218	25.532
5	10.75	11.099	13.931	27.185
7.5	12.558	12.934	16.027	28.546
10	14.030	14.433	17.725	29.691
Rigid	16.033	16.468	20.008	31.567

Table C.4: Critical live load in kN/m from the first positive global eigenmode of the truss where k_{ax} is given in kN/m and k_{rz} in kNm/rad.

Rotational Stiffness Z	Stiffness X 100	Stiffness X 1 000	Stiffness X Rigid
0	54.570	102.750	Local
0.1	54.587	102.613	Local
1	55.118	102.958	Local
2.5	54.975	103.018	Local
5	55.331	103.262	Local
7.5	55.649	103.417	Local
10	55.930	103.525	Local
Rigid	56.516	103.775	Local

Table C.5: Critical live load in kN/m from the first negative global eigenmode of the truss where k_{ax} is given in kN/m and k_{rz} in kNm/rad.

Rotational Stiffness Z	Stiffness X 0	Stiffness X 0.1	Stiffness X 1	Stiffness X 10
0	-12.597	-12.718	-13.659	-17.807
0.1	-12.753	-12.876	-13.838	-18.067
1	-14.010	-14.156	-15.286	-20.112
2.5	-15.711	-15.885	-17.233	-22.691
5	-17.891	-18.101	-19.708	-25.644
7.5	-19.588	-19.817	-21.606	-27.673
10	-20.962	-21.216	-23.140	-29.187
Rigid	-22.838	-23.117	-25.201	-31.423

Table C.6: Critical live load in kN/m from the first negative global eigenmode of the truss where k_{ax} is given in kN/m and k_{rz} in kNm/rad.

Rotational Stiffness Z	Stiffness X 100	Stiffness X 1 000	Stiffness X Rigid
0	-21.298	-22.319	-22.516
0.1	-21.583	-22.447	-22.793
1	-23.829	-24.679	-24.856
2.5	-25.908	-26.873	-27.056
5	-28.584	-29.341	-29.559
7.5	-30.032	-31.018	-31.266
10	-31.502	-32.291	-32.774
Rigid	-32.501	-33.356	-33.965

Table C.7: Critical live load in kN/m corresponding to eigenmode according to figure 4.20, where k_{ax} is given in kN/m and k_{rz} in kNm/rad.

Rotational Stiffness Z	Stiffness X 0	Stiffness X 0.1	Stiffness X 1	Stiffness X 10
0	5.166	5.400	7.356	20.868
0.1	5.328	5.566	7.548	21.201
1	6.648	6.911	9.105	23.860
2.5	8.442	8.741	11.218	27.123
5	10.75	11.099	13.931	36.240
7.5	12.558	12.934	16.027	39.636
10	14.030	14.433	17.725	42.609
Rigid	16.033	16.468	20.008	47.202

Table C.8: Critical live load in kN/m corresponding to eigenmode according to figure 4.20, where k_{ax} is given in kN/m and k_{rz} in kNm/rad. No found value is represented by '-'. '.

Rotational Stiffness Z	Stiffness X 100	Stiffness X 1 000	Stiffness X Rigid
0	84.509	-	-
0.1	85.344	-	-
1	92.515	-	-
2.5	101.105	-	-
5	112.407	-	-
7.5	-	-	-
10	-	-	-
Rigid	-	-	-